metals

MDPI

Article

Use of Electrochemical Noise for the Study of Corrosion by Passivated CUSTOM 450 and AM 350 Stainless Steels

Facundo Almeraya-Calderon [1,*], Miguel Villegas-Tovar [1], Erick Maldonado-Bandala [2], Maria Lara-Banda [1], Miguel Angel Baltazar-Zamora [2], Griselda Santiago-Hurtado [3], Demetrio Nieves-Mendoza [2], Luis Daimir Lopez-Leon [4], Jesus Manuel Jaquez-Muñoz [5], Francisco Estupiñán-López [1] and Citlalli Gaona-Tiburcio [1,*]

1 Universidad Autónoma de Nuevo León, FIME, Centro de Investigación e Innovación en Ingeniería Aeronáutica (CIIIA), San Nicolás de los Garza 66455, Mexico; miguel.villegastvr@uanl.edu.mx (M.V.-T.); maria.laraba@uanl.edu.mx (M.L.-B.); francisco.estupinanlp@uanl.edu.mx (F.E.-L.)
2 Facultad de Ingeniería Civil, Universidad Veracruzana, Xalapa 91000, Mexico; erimaldonado@uv.mx (E.M.-B.); mbaltazar@uv.mx (M.A.B.-Z.); dnieves@uv.mx (D.N.-M.)
3 Facultad de Ingeniería Civil, Universidad Autónoma de Coahuila, Torreón 27276, Mexico; santiagog@uadec.edu.mx
4 Área Académica de Ingeniería y Arquitectura, Universidad Autónoma del Estado de Hidalgo, Carretera Pachuca-Tulancingo Km. 4.5., Pachuca 42082, Mexico; luis_lopez@uaeh.edu.mx
5 Instituto de Ingeniería y Tecnología, Universidad Autónoma de Ciudad Juárez, Ciudad Juárez 32310, Mexico; jesus.jaquezmn@uanl.edu.mx
* Correspondence: facundo.almerayacld@uanl.edu.mx (F.A.-C.); citlalli.gaonatbr@uanl.edu.mx (C.G.-T.)

Abstract: Precipitation-hardening stainless steels, like AM 350 and Custom 450, are extensively utilized in various aerospace applications. The latter steel is utilized for applications needing great strength and corrosion resistance. In contrast, the former steel has a good corrosion resistance and moderate strength. The purpose of this study was to analyze transient frequencies in the electrochemical noise of Custom 450 and AM 350 stainless steels that had been passivated for 60 and 90 min at 25 and 49 °C using baths of citric and nitric acid and then immersed in solutions containing 1% sulfuric acid (H_2SO_4) and 5% sodium chloride (NaCl). The potentiodynamic polychromatic curves employed electrochemical techniques and noise (EN) based on the ASTM-G5 and G199 standards. Two methods of data analysis were applied concerning EN: the domain of frequencies (power spectral density, PSD) and the time–frequency domain (Hilbert-Huang Transform). The PHSS passivated in citric acid indicated current densities in the H_2SO_4 solution between 10^{-2} and 10^{-3} mA/cm^2, while those in the NaCl solution were recorded around 10^{-4} and 10^{-5} mA/cm^2. The citric acid functions as a passivating agent. The results of the electrochemical noise analysis show that the PHSS passivated in nitric acid displayed a greater corrosion resistance. Moreover, there is a tendency for PHSS to be passivated in nitric acid to corrode locally.

Keywords: corrosion; potentiodynamic polarization; electrochemical noise; precipitation hardening; stainless steels

check for updates

Citation: Almeraya-Calderon, F.; Villegas-Tovar, M.; Maldonado-Bandala, E.; Lara-Banda, M.; Baltazar-Zamora, M.A.; Santiago-Hurtado, G.; Nieves-Mendoza, D.; Lopez-Leon, L.D.; Jaquez-Muñoz, J.M.; Estupiñán-López, F.; et al. Use of Electrochemical Noise for the Study of Corrosion by Passivated CUSTOM 450 and AM 350 Stainless Steels. *Metals* **2024**, *14*, 341. https://doi.org/10.3390/met14030341

Academic Editor: Francesca Borgioli

Received: 18 February 2024
Revised: 13 March 2024
Accepted: 13 March 2024
Published: 16 March 2024

1. Introduction

Stainless steels can improve their corrosion resistance if they undergo a chemical treatment called passivation [1,2].

Stainless steels are alloys that contain at least 11% chromium and other alloying elements. These steels provide excellent corrosion resistance and are classified into five groups according to their microstructural phases [3–5]. In the aeronautical sector, stainless steels such as precipitation-hardened (PH) steels are used. These steels' superior qualities—such as their strong corrosion resistance, low density, and mechanical resistance—make them suitable for usage in particular components [4]. Both martensitic and semi-austenitic PHSSs (precipitation-hardened stainless steels) exist. Austenitic stainless steel after annealing

is essentially the semi-austenitic kind. After this, a heat treatment is applied, causing the austenitic phase to change into the martensitic phase in preparation for the following hardening process [5]. Some of the most used PH steels in the aerospace sector are 17-7 PH, 17-4 PH, Custom 450 (Carpenter Technology Corporation, Philadelphia, PA, USA), and AM 350 (ATI Materials, Dallas, TX, USA), and are used to manufacture the turbine blades, rotors, and shafts. 15-5 PH steel (Penn Stainless Products, Inc., Bucks County, PA, USA) is used in structural components [6,7].

The thin, compact, invisible, and protective oxide film naturally forming on the stainless steel's surface accounts for its high corrosion resistance. A chemical treatment called passivation allows for the growth of the oxidation film on the surface of the stainless steel, thus improving its corrosion resistance, given that the oxide film is continuous, compact, and adherent. Stainless steels must have a chromium amount greater than 11%, and the passivity will be greater at a higher concentration [8–13].

As a substitute, the citric acid ($C_6H_8O_7$) passivation of aircraft stainless steel parts was first investigated in 2003. The Boeing Company began this task between 2008 and 2011. NASA (National Aeronautics and Space Administration) and the US Department of Defense (DoD) (Washington, DC, USA) began to passivate stainless steels in citric acid to improve their corrosion resistance. Passivation commonly uses nitric acid (NHO_3), a strong and toxic oxidant. Citric acid is an alternative for this type of treatment due to its low toxicity and being environmentally friendly. It is also used in low concentrations of around 10%, while nitric acid is usually used in concentrations of 40% [14,15].

Electrochemical techniques like potentiodynamic polarization (PP), electrochemical noise (EN), and electrochemical impedance spectroscopy (EIS) are used in corrosion research to assess passivated stainless steel. These techniques help us understand the corrosion mechanism and dynamics of the system under study.

Spontaneous changes in the potential and current that occur during a corrosion process are referred to as the electrochemical noise. Small changes in the electrical charges on an electrode are caused mainly by electrochemical cathodic and anodic reactions during the electrochemical corrosion process [16–19]. Electrical signals known as transients are connected to anodic and cathodic reactions in response to the creation and spread of pitting or the rupture and re-passivation of the passive film; the former process is stochastic, while the latter is deterministic [20,21]. Several techniques can be used to analyze EN data. The most popular ones are probably those that deal with the frequency domain (power spectral density, for instance), the time domain (statistical techniques like kurtosis, skewness, and localization index (LI), among others), and the time–frequency domain [22–25]. It has been discovered, in recent years, that a statistical analysis is limited in identifying the corrosion type present during the process. In the time–frequency domain, innovative techniques like Wavelet and Hilbert–Huang Transform (HHT) are employed to reduce the uncertainty of the statistical study's findings. They examine chaotic signals of electrochemical noise to identify the corrosion mechanism [26–31].

El-Taib Heakal et al.'s 2004 study [32] on the electrochemical behaviors of molybdenum-containing stainless steels in the presence of aerated and reaerated solutions supported the hypothesis that the alloying elements were responsible for the pH drop. In 2007, the same authors [33] investigated the stability of the growth of passivation films in stainless steels, where alloying elements such as molybdenum provide that stability. Using electrochemical techniques like electrochemical noise and potentiodynamic polarization curves, other studies in the literature have made it possible to evaluate stainless steels like the real SS304 and the precipitation-hardened 15-5 PH and 17-4 PH in order to determine the corrosion kinetics of the passive film [22,34]. When steel is passivated, its pitting potential in nitric acid rises [23]. According to Marcelin et al.'s [24] investigation, the passive film characteristics governed the electrochemical process in the corrosion of martensitic stainless steel. Hydrogen diffusion, microstructural characterization, and mechanical behavior have been the main topics of recent studies on PHSSs [25,35]. Using electrochemical techniques, including potentiostatic polarization, electrochemical noise, potentiodynamic polarization,

and electrochemical impedance spectroscopy, Gaona, Samaniego, and Villegas [36–38] have investigated the corrosion behaviors of PHSSs in acid baths.

Recent studies on corrosion in stainless steels have concentrated on real steel. Little research has been conducted on PHSSs. Thus, it is critical to understand electrochemical corrosion in the electrolytes that are often used in airplanes, such as in industrial, urban, and marine environments [39,40].

The present work aims to study the frequency analysis of transients using electrochemical noise measurements of Custom 450 and AM 350 stainless steels that have been passivated in citric ($C_6H_8O_7$) and nitric (HNO_3) acid baths for 60 and 90 min at 25 and 49 °C, respectively, and exposed to 1% sulfuric acid (H_2SO_4) and 5% sodium chloride (NaCl) solutions. Potentiodynamic polarization curves and electrochemical noise were the electrochemical methods employed.

2. Materials and Methods

2.1. Materials

The stainless steels used were Custom 450 (AMS 5773) and AM 350 (AMS 5548) in the shape of cylindrical bars (AMS Aerospace Material Specifications). Table 1 lists the nominal chemical makeup of various PHSSs.

Table 1. The chemical composition of the used stainless steels (wt.%).

Elements	Stainless Steel Alloys	
	Custom 450	**AM 350**
Fe	Balance	Balance
C	≤0.05	0.07–0.11
Cr	14.0–16.0	16.0–17.0
Ni	5.0–7.0	4.0–5.0
Mo	0.50–1.0	2.50–3.25
Mn	1.00	0.50–1.25
N	≤0.1	0.07–0.13
Si	1.00	≤0.50
S	0.030	0.030
Cu	1.25–1.75	–
Ti	0.90–1.40	–
Nb	0.5–0.75	–

The specimens were obtained from cylindrical bars with thicknesses of 0.5 cm, according to ASTMA380 [41]. Subsequently, all the specimens were prepared using the metallography technique ASTM E3 [42] and were roughed with silica carbide (SiC) sandpaper. The samples were then ultrasonically cleaned with ethyl alcohol to give them a clearer, impurity-free surface.

An optical metallurgical microscope (OM, Olympus, Hamburg, Germany) was used to determine the microstructures of the PHSSs.

2.2. Passivation Process

Based on the SAE/ASM2700 and ASTM G967 guidelines, the factors of the passivation process were controlled [43,44]. The passivation process consisted of the following steps, see Figure 1 [2,7,36–38]:

(a) Pretreatment stage: The stainless steel was degreased and pickled for five seconds at 25 °C in a 50-weight percent hydrochloric acid (HCl) solution (analytical grade reagents). The steel was then rinsed in distilled water.
(b) Passivation stage: a total of two passivation baths using solutions of distilled water (analytical grade reagents), citric acid (55% v), and nitric acid (20% v) were utilized.
(c) The two temperatures were 25 and 49 °C.
(d) The samples were immersed in the solutions for 60 and 90 min.

(e) Final stage: the samples were rinsed in distilled water.
(f) A total of 64 trials using the two PHSSs were conducted.

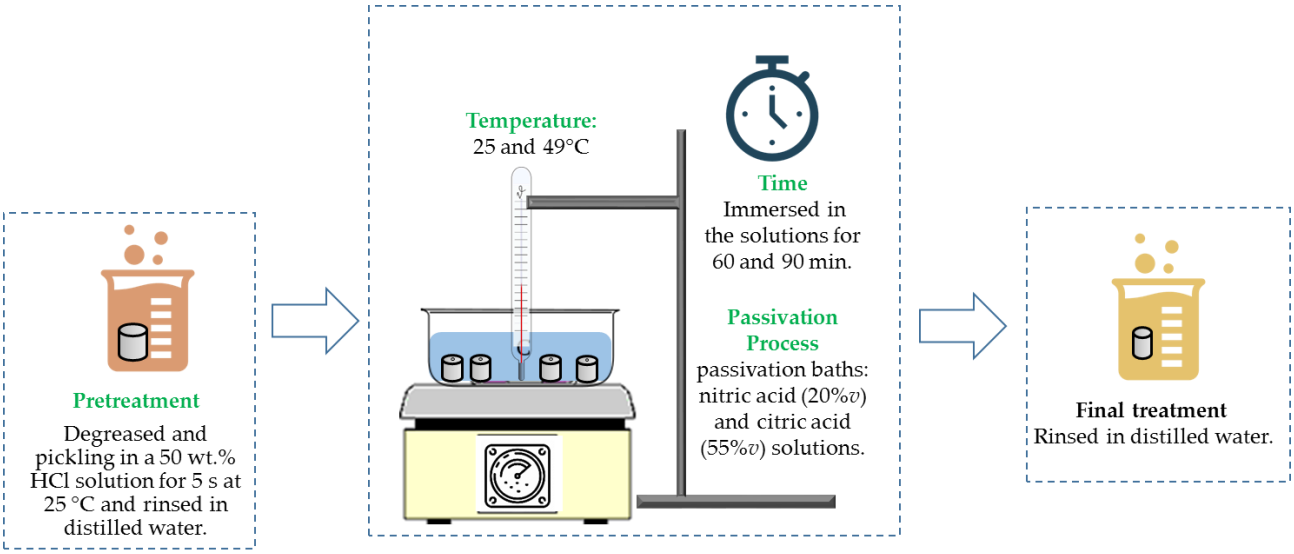

Figure 1. Diagram of the passivation process of PHSSs in acid baths.

2.3. Electrochemical Measurements

The corrosion kinetics of PHSSs were ascertained using the electrochemical methods of potentiodynamic polarization (PP) and electrochemical noise (EN). A three-electrode electrochemical cell configuration was used for the corrosion tests, which were carried out in duplicate at room temperature using a Potentiostat/Galvanostat/ZRA (produced by Solartron 1287A, Bognor Regis, UK). The tests were evaluated in solutions containing 1% and 5% sulfuric acid (H_2SO_4) and sodium chloride (NaCl).

As per the ASTM G5-11 standard [45–47], potentiodynamic polarization (PP) tests were performed over −1.0 and 1.2 V of OCP, with a scan rate of 0.06 V/min applied. The electrochemical cell employed was one of the three electrodes: the working electrode (material to analyze), a saturate calomel electrode (SCE) as the reference electrode, and a platinum wire as the counter electrode.

The EN measurements complied with the ASTM G199-09 standard [48]; 1024 data points were scanned at one data point per second for each set of EN measurements. Before a fast Fourier transform (FTT) was applied to convert the power spectral density (PSD) data to the frequency domain, a Hann window was utilized. The EN signal's intrinsic functions (IMF) were derived using the Hilbert–Huang Transform (HHT) EN analysis. Then, using the empirical decomposition method (EMD), the instantaneous frequencies were shown using the Hilbert spectrum. A program created in Math Works' MATLAB 2018a software (Natick, MA, USA) was used to process the EN data [48–50].

3. Results

3.1. Microstructures of PHSSs

The microstructures of the PHSSs, as determined using optical microscopy, are shown in Figure 2. For the steel Custom 450, this alloy showed a martensitic (α') phase. In contrast, the AM 350 semi-austenitic SS showed austenite (γ) and delta (δ) ferrite phases in its microstructure, respectively.

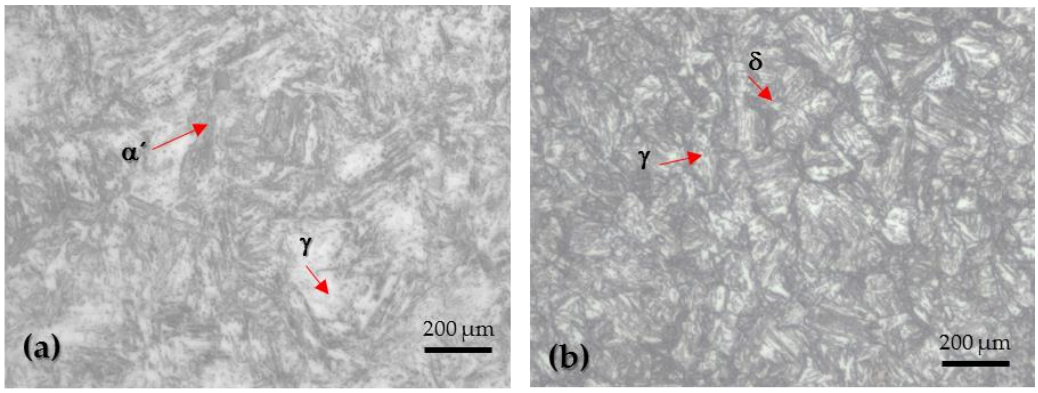

Figure 2. OM microstructures of PHSSs. (**a**) Custom 450 and (**b**) AM 350.

3.2. Potentiodynamic Polarization

The corrosion kinetics behaviors of the passivated steels were obtained through the potentiodynamic polarization curves, where electrochemical parameters such as the corrosion current density, i_{corr} (µA/cm^2); corrosion potential, E_{corr} (mV); corrosion rate (mm/yr); anodic Tafel slope (β_a); and cathodic Tafel slope (β_c) were obtained using the Tafel extrapolation method [50–52]. The potentiodynamic polarization curves refer to the relationship curve between the electrode potential and polarization current density and include the anode and cathode polarization curves. The linear area of the two polarization curves is extended to a point where the intersection is the corresponding current density (i_{corr}). The PPC for the PHSSs passivated in acid baths at 25 and 49 °C for 60 and 90 min while submerged in NaCl and H_2SO_4 solutions are displayed in Figures 3 and 4.

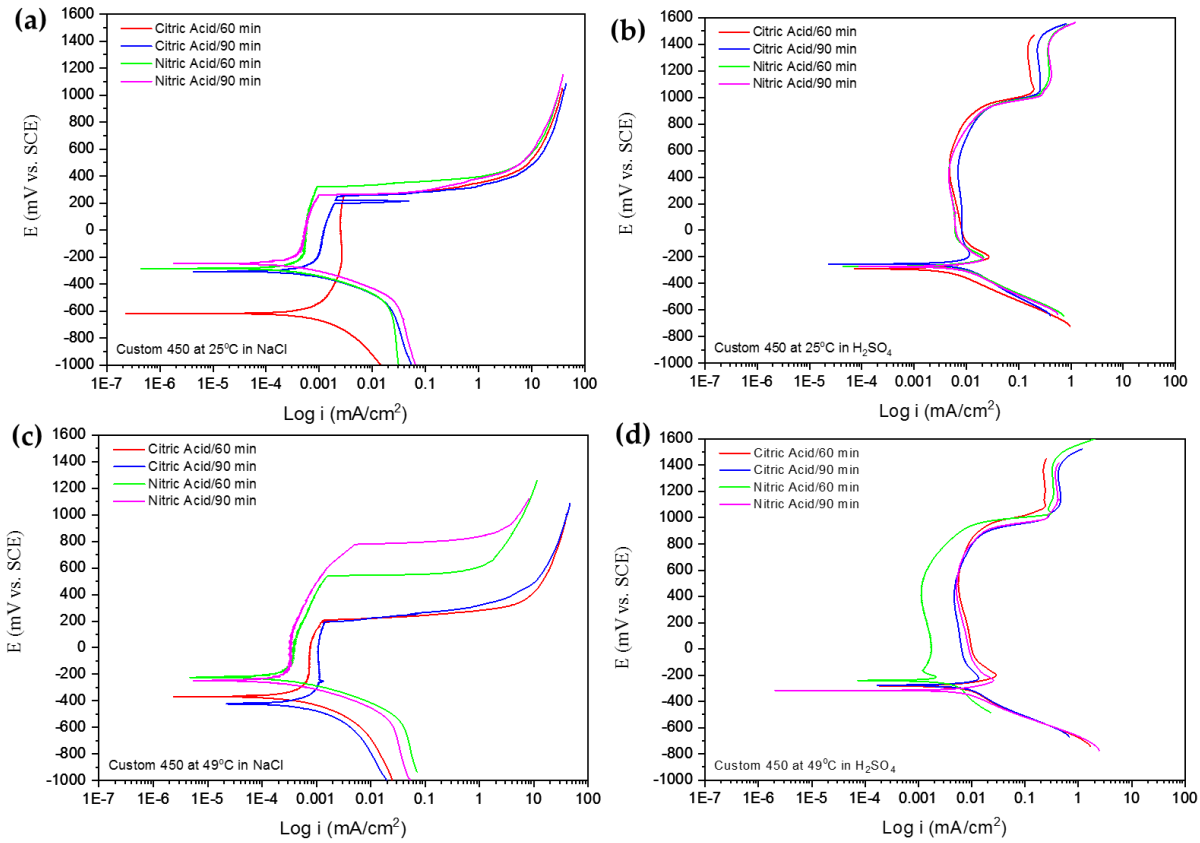

Figure 3. Potentiodynamic polarization curves for Custom 450 samples passivated in citric and nitric acids at 25 and 49 °C for 60 and 90 min: (**a**,**c**) NaCl and (**b**,**d**) H_2SO_4 solutions.

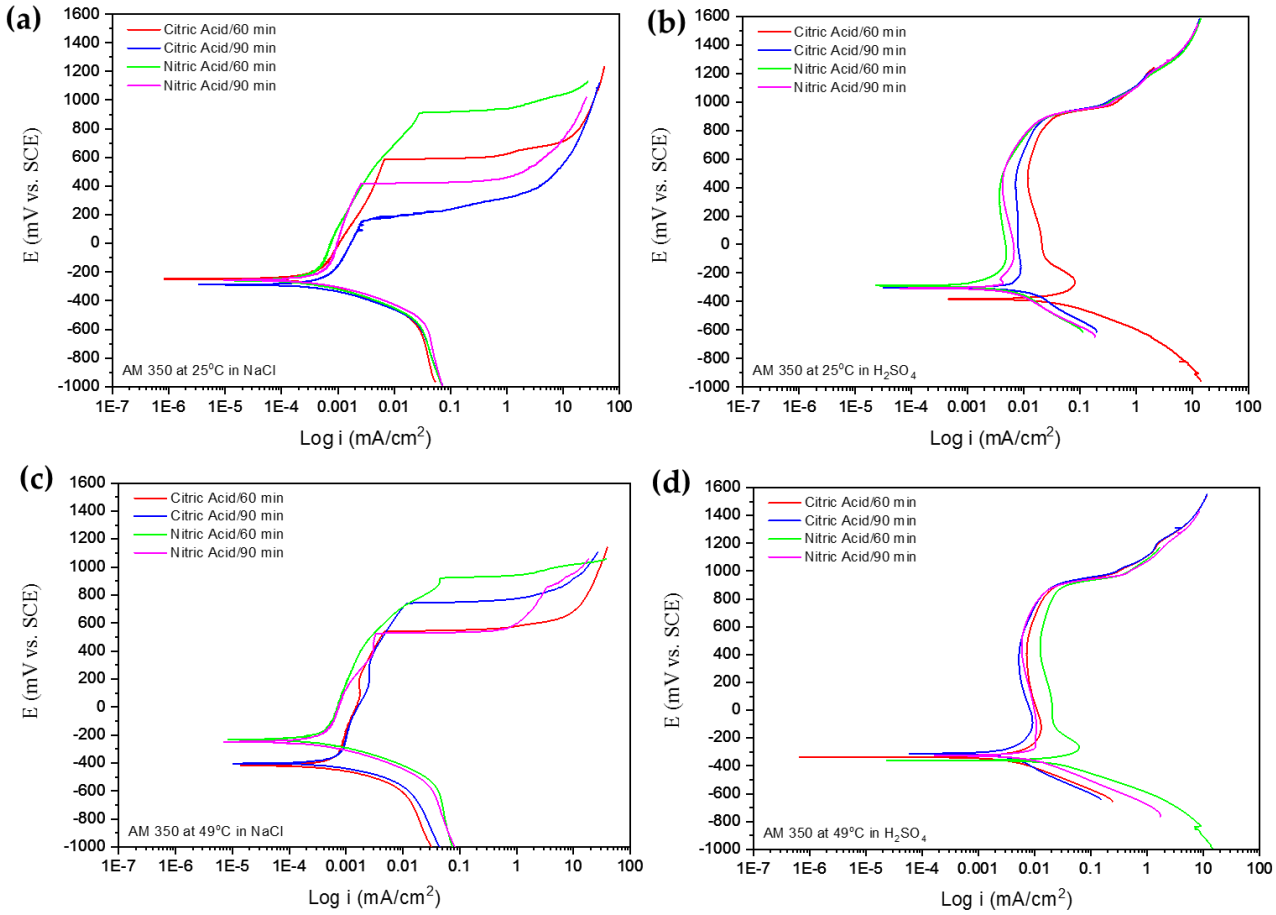

Figure 4. Potentiodynamic polarization curves for AM 350 samples passivated in citric and nitric acids at 25 and 49 °C for 60 and 90 min: (**a**,**c**) NaCl and (**b**,**d**) H_2SO_4 solutions.

The PPCs, which show a mixed control by activation in the anodic reactions as the formation of oxides that lead to passivation, typically illustrates the corrosion potential vs. the current's logarithm. Tables 2 and 3 provide an overview of the electrochemical characteristics derived from potentiodynamic polarization (PP) curves.

The PPCs for passivated Custom 450 samples are shown in Figure 3a–d, where the samples are exposed to solutions containing sulfuric acid, sodium chloride, and citric and nitric acids at 25 and 49 °C for 60 and 90 min. Most of the time, the corrosion potential (E_{corr}) was close to −270 mV vs. the SCE. Nevertheless, at 25 °C, the corrosion potential in NaCl was −619 mV vs. the SCE. Every single passivated PHSS sample reacted with a stable passivation range in both solutions when subjected to the sulfuric acid solution at 25 and 49 °C temperatures. In the PHSS Custom 450, the materials subjected to sodium chloride exhibited pseudo-passivation followed by transpassivation. At the same time, all samples demonstrated secondary passivation when sulfuric acid was added. The electrochemical data are reported in Table 2. The corrosion current densities (i_{corr}) of the PHSS samples, when passivated in citric acid and exposed to sulfuric acid, are 10^{-3} mA/cm^2, whereas in NaCl, they are significantly lower, at 10^{-4} mA/cm^2 [36,53].

The PPCs for PHSSs that were obtained from nitric acid baths at 25 and 49 °C for 60 and 90 min while the passivated PHSSs were exposed to H_2SO_4 and NaCl solutions are shown in Figure 4a–d. The PPCs for passivated AM 350 samples in citric and nitric acids at 25 and 49 °C for 60 and 90 min with exposure to sulfuric acid and sodium chloride solutions are shown in Figure 4a–d. The 558–1049 mV region was where the anodic and cathodic branches showed activation. The corrosion potential (E_{corr}) was mostly approximately −300 mV. When sulfuric acid solutions were supplied, all passivated PHSS samples

produced a steady passivation range at 25 and 49 °C. The passivated AM 350 samples were displayed after pseudo-passivation in a sodium chloride solution and transpassivation for 60 and 90 min at 25 and 49 °C, respectively. Table 3 lists the electrochemical parameters for the PHSS samples that were passivated in citric acid and exposed to sulfuric acid. Their corrosion current densities (i_{corr}) range from 10^{-2} to 10^{-4} mA/cm^2, while in NaCl, they have significantly lower current densities of 10^{-4} to 10^{-5} mA/cm^2.

Table 2. Obtained electrochemical parameters for Custom 450 samples passivated in citric and nitric acids for 60 and 90 min with exposure to H_2SO_4 and NaCl solutions.

Acid Bath	Time (min)	Temp. (°C)	E_{corr} (mV vs. SCE)	E_{pit} (mV)	i_{corr} (mA/cm^2)	β_a (mV/decade)	β_c (mV/decade)	i_{pass} (mA/cm^2)	Passivation Range (mV)	Corrosion Rate (mm/yr)
Immersed in 1 wt. % H_2SO_4 Solution										
Citric	60	25	−289	768	9.79×10^{-4}	146.38	76.38	8.9×10^{-3}	722	1.10×10^{-2}
		49	−294	916	7.37×10^{-3}	169.89	144.78	1.09×10^{-2}	778	8.28×10^{-2}
Nitric		25	−276	936	8.29×10^{-3}	181.4	73.34	6.34×10^{-2}	711	9.3×10^{-2}
		49	−253	937	3.46×10^{-3}	73.42	30.79	1.03×10^{-3}	878	3.88×10^{-2}
Citric	90	25	−254	930	1.12×10^{-3}	160.56	94.12	8.61×10^{-2}	722	1.42×10^{-2}
		49	−246	939	4.80×10^{-3}	86.23	123.10	7.58×10^{-2}	758	5.30×10^{-2}
Nitric		25	−250	934	5.73×10^{-3}	208.16	71.51	6.69×10^{-2}	883	6.43×10^{-2}
		49	−317	899	6.17×10^{-4}	96.99	66.00	1.15×10^{-2}	911	8.39×10^{-3}
Immersed in 5 wt. % NaCl Solution										
Citric	60	25	−619	251	3.04×10^{-4}	175.11	91.25	2.42×10^{-3}	518	3.41×10^{-3}
		49	−367	203	1.13×10^{-4}	110.22	87.75	6.69×10^{-4}	304	1.2×10^{-3}
Nitric		25	−284	315	2.7×10^{-4}	118.7	105.56	5.32×10^{-4}	485	3.10×10^{-3}
		49	−224	536	4.7×10^{-5}	46.42	69.80	3.09×10^{-4} *	673 *	5.36×10^{-4}
Citric	90	25	−308	311	1.55×10^{-4}	103.37	67.07	8.62×10^{-4} *	422 *	1.74×10^{-3}
		49	−430	537	1.19×10^{-4}	103.95	62.71	1.06×10^{-3}	445	1.34×10^{-3}
Nitric		25	−250	260	7.45×10^{-5}	87.59	61.74	4.41×10^{-4} *	405 *	8.34×10^{-5}
		49	−249	777	3.25×10^{-5}	63.33	69.69	3.1×10^{-4}	212	3.66×10^{-4}

* pseudo-passivation.

Table 3. Obtained electrochemical parameters for AM 350 samples passivated in citric and nitric acids for 60 and 90 min with exposure to H_2SO_4 and NaCl solutions.

Acid Bath	Time (min)	Temp. (°C)	E_{corr} (mV vs. SCE)	E_{pit} (mV)	i_{corr} (mA/cm^2)	β_a (mV/decade)	β_c (mV/decade)	i_{pass} (mA/cm^2)	Passivation Range (mV)	Corrosion Rate (mm/yr)
Immersed in 1 wt. % H_2SO_4 Solution										
Citric	60	25	−378	586	5.02×10^{-3}	68.7	93.61	2.2×10^{-2}	737	5.64×10^{-2}
		49	−329	840	5.16×10^{-4}	106.85	39.96	1.29×10^{-2}	680	5.80×10^{-3}
Nitric		25	−290	874	3.37×10^{-4}	61.15	53.17	4.7×10^{-3}	575	3.79×10^{-3}
		49	−356	882	1.03×10^{-2}	118.43	111.5	2.15×10^{-2}	994	1.11×10^{-1}
Citric	90	25	−299	876	1.39×10^{-3}	64.07	69.22	5.8×10^{-3}	698	1.56×10^{-2}
		49	−320	885	1.14×10^{-3}	62.09	158.57	5.7×10^{-3}	596	1.28×10^{-2}
Nitric		25	−302	895	4.46×10^{-4}	64.30	58.05	6.6×10^{-3}	735	5.01×10^{-3}
		49	−322	737	1.56×10^{-3}	66.79	81.24	1.01×10^{-2}	847	1.75×10^{-2}
Immersed in 5 wt. % NaCl Solution										
Citric	60	25	−251	586	5.92×10^{-5}	32.12	51.13	7.8×10^{-3} *	711 *	6.65×10^{-4}
		49	−418	539	7.24×10^{-5}	52.88	40.16	7.7×10^{-4} *	849 *	8.13×10^{-4}
Nitric		25	−267	906	4.78×10^{-4}	49.12	74.71	5.4×10^{-3} *	1049 *	5.37×10^{-3}
		49	−228	921	1.39×10^{-4}	76.94	76.28	6.5×10^{-4} *	1038 *	1.56×10^{-3}
Citric	90	25	−297	910	3.43×10^{-4}	191.4	103.84	7.3×10^{-4} *	351 *	3.85×10^{-3}
		49	−406	925	9.99×10^{-5}	51.15	69.17	8.92×10^{-4} *	1048 *	1.11×10^{-3}
Nitric		25	−253	417	2.04×10^{-4}	92.59	94.52	7.1×10^{-4} *	558 *	2.29×10^{-3}
		49	−251	522	1.27×10^{-4}	89.48	79.54	5.7×10^{-3} *	671 *	1.43×10^{-3}

* pseudo-passivation.

The citric and nitric acid-passivated Custom 450 and AM 350, where the steels are exposed to sulfuric acid and sodium chloride solutions, form more stable layers when followed by transpassivation and secondary passivation. The electrochemical parameters obtained from these measurements are illustrated in Tables 2 and 3.

3.3. Electrochemical Noise

Since there is a correlation between the EN signal (with the polynomial filter applied), the PSD analysis requires a transformation of the time-domain EN to the frequency domain using FFT. Equations (1) and (2) are then calculated once the spectral density is calculated [54–56], where R_{xx} (m) is related to a signal correlation.

$$R_{xx}(m) = \frac{1}{N}\sum_{n=0}^{N-m-1} x(n)\cdot x(n+m), \text{when values are from } 0 < m < N \quad (1)$$

$$\Psi_x(k) = \frac{\gamma\cdot t_m}{N}\cdot\sum_{n=1}^{N}(x_n - \overline{x}_n)\cdot e^{\frac{-2\pi kn^2}{N}} \quad (2)$$

The PSD is interpreted using the limit frequency to cut the frequency as a basis. The cut frequency indicates a slope's start and end, which helps determine the corrosion mechanism. Information regarding the sample representation following pitting is provided by the cut frequency. The slope is expressed for Equation (3) and is defined by β_x [57].

$$\log\Psi_x = -\beta_x \log f \quad (3)$$

The frequency zero limit (ψ_0) provides information on the material disintegration, as the PSD is connected to the entire amount of energy in the system. It is crucial to make clear that the current PSD is the only one with material dissolution. The following Table 4, adjusted to decibels, was suggested by Mansfeld et al. [58–61] in 1998 to determine the corrosion phenomena on the material surface.

Table 4. Electrochemical parameters (β intervals to indicate the type of corrosion).

β Intervals	Corrosion Type					
	Uniform		Pitting		Passive	
	Minimum	Maximum	Minimum	Maximum	Minimum	Maximum
dB(V)·Decade^{-1}	0	−7	−20	−25	−15	−25
dB(A)·Decade^{-1}	0	−7	−7	−14	−1	1

Figure 5 shows the PSD graphics of the Custom 450 alloy when it was passivated at 25 and 49 °C in different environments. Figure 5a shows the results of Custom 450 passivated at 25 °C exposed to NaCl. The passivation in citric acid after 90 min presented a higher Ψ^0 (−65 dBi), indicating a higher corrosion kinetic. On the other hand, in Figure 5b, the nitric acid passivation of 90 min presented the lower corrosion kinetic (−110 dBi). For that reason, passivation can be considered one of the most resistant mechanisms. The sample was anodized in nitric acid when the passivated alloys were exposed to H_2SO_4 at 25 °C. At the same time, a 60 min exposure resulted in a lower energy demand (−130 dBi). The other samples presented similar values of Ψ^0, meaning the corrosion kinetics are high in this environment. Only the samples citric/90min and nitric/60min presented uniform corrosion (see Table 5) when exposed to H_2SO_4.

Figure 5c,d show the passivated behavior of Custom 450 at 49 °C. When exposed to NaCl, the sample nitric/60 min showed higher corrosion kinetics (56 dBi). Meanwhile, the citric/60 min sample presented a lower value of −82 dBi. When the samples were exposed to H_2SO_4, only the citric/90min sample presented a higher Ψ^0 (−100); the rest presented similarly in the corrosion kinetics. All the passivated samples exposed to H_2SO_4 presented slope values corresponding to uniform corrosion (see Table 6).

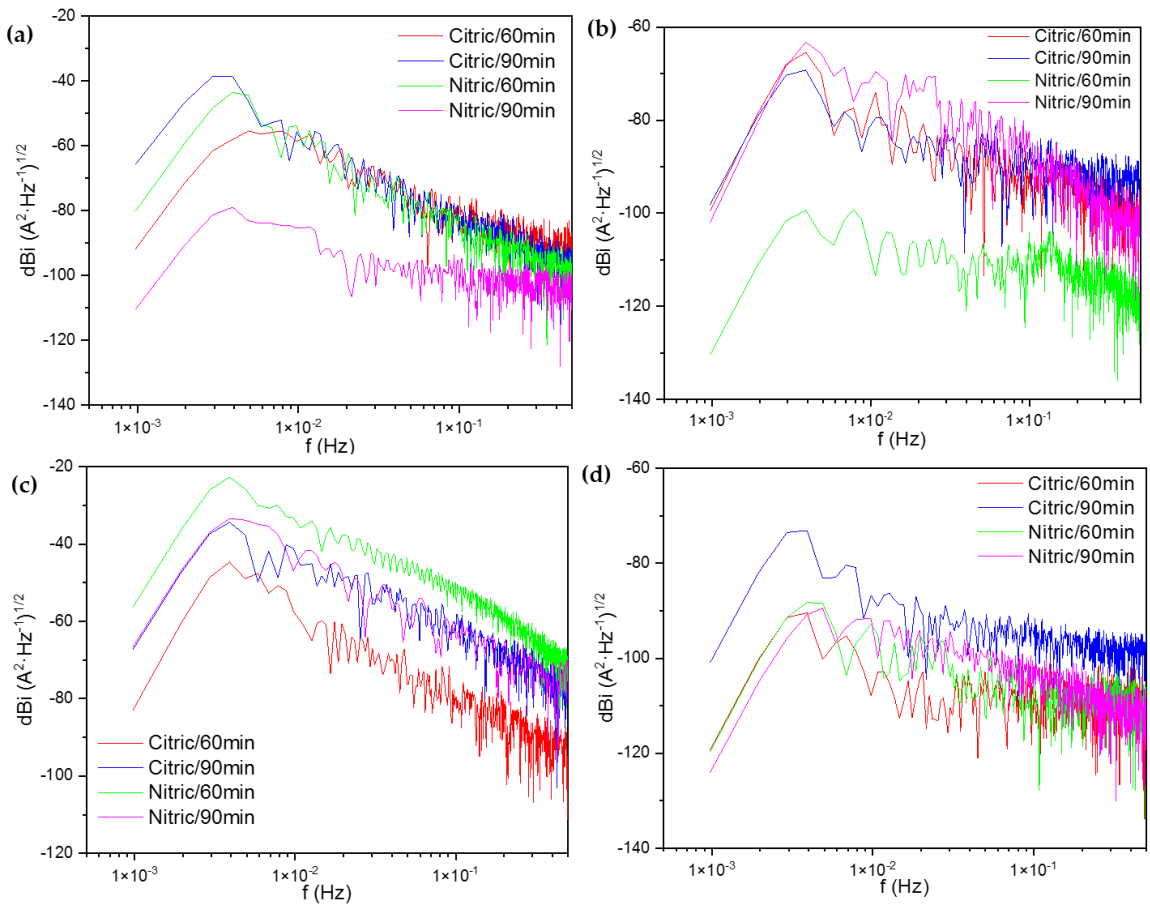

Figure 5. PSDs in currents for Custom 450 passivated at 25 °C exposed to (**a**) NaCl and (**b**) H_2SO_4 solutions and Custom 450 passivated at 49 °C exposed to (**c**) NaCl and (**d**) H_2SO_4 solutions.

Table 5. The parameters were obtained using PSD and Z_n for PHSSs passivated and exposed to the NaCl solution.

Electrolyte	PHSS	Acid Bath	Temperature (°C)	Time (Minutes)	Slope (β)	Ψ^0 (dBi)	Z_n (Ω·cm^2)
NaCl	Custom 450	Citric	25	60	−14	−91	1103
				90	−20	−65	1221
			49	60	−17	−82	5532
				90	−17	−67	2537
		Nitric	25	60	−20	−80	2865
				90	−5	−110	126,654
			49	60	−20	−56	16,487
				90	−17	−66	14,971
	AM 350	Citric	25	60	−16	−61	6619
				90	−16	−58	11,814
			49	60	−17	−82	21,871
				90	−18	−67	1103
		Nitric	25	60	−17	−80	20,786
				90	−13	−97	41,784
			49	60	−20	−68	15,002
				90	−18	−66	5768

Table 6. Parameters obtained using PSD and Z_n for PHSSs passivated and exposed to H_2SO_4 solution.

Electrolyte	PHSS	Acid Bath	Temperature (°C)	Time (Minutes)	Slope (β)	Ψ^0 (dBi)	Z_n ($\Omega \cdot cm^2$)
H_2SO_4	Custom 450	Citric	25	60	−9	−99	50,805
				90	−4	−98	23,982
			49	60	−1	−119	59,557
				90	−5	−100	15,931
		Nitric	25	60	−5	−130	1,410,107
				90	−16	−119	29,020
			49	60	−4	−101	57,061
				90	−8	−124	30,162
	AM 350	Citric	25	60	−6	−114	5768
				90	−4	−101	5749
			49	60	−5	−88	11,824
				90	−11	−106	106,720
		Nitric	25	60	−13	−104	81,021
				90	−12	−117	243,070
			49	60	−12	−112	110,839
				90	0	−124	52,219

Figure 6 shows the passivated samples of the alloy AM 350. Figure 6a shows the behaviors of the passivated samples when exposed to NaCl. The sample nitric/90 min presented the lower Ψ^0 value (−97 dBi), indicating lower corrosion kinetics than the samples passivated in citric acid that presented higher values. This behavior was also presented when the samples were exposed to H_2SO_4; the samples passivated in nitric acid obtained a better performance in the corrosion kinetics.

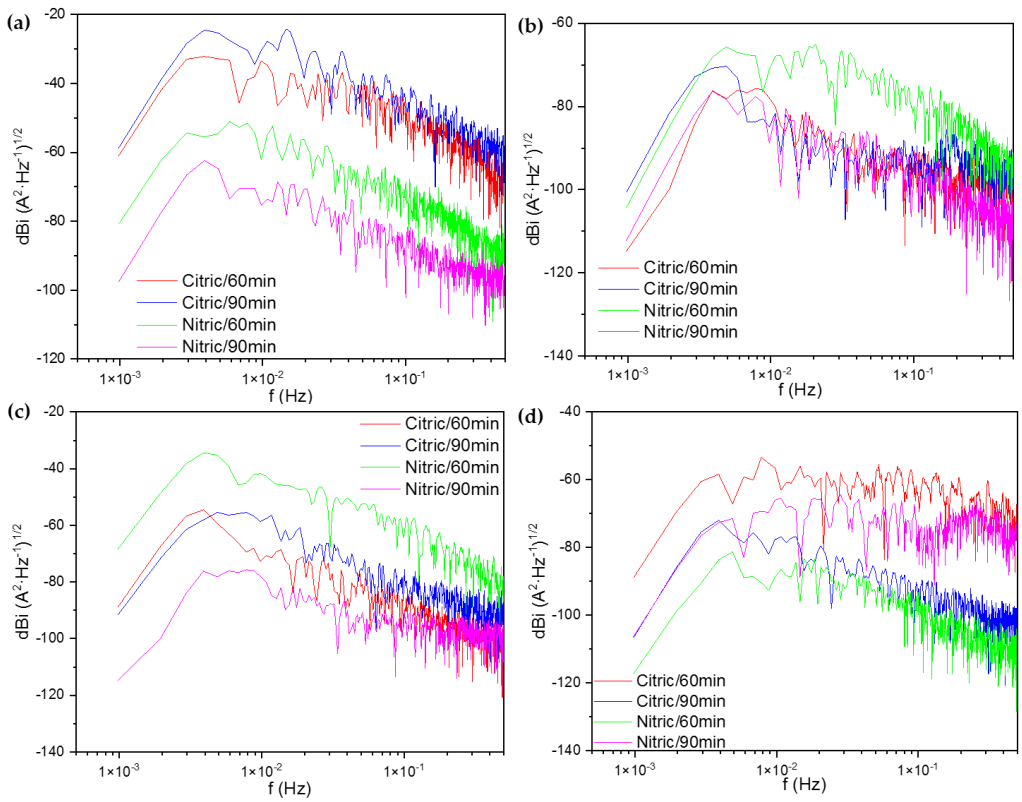

Figure 6. PSDs in currents for AM 350 passivated at 25 °C exposed to (**a**) NaCl and (**b**) H_2SO_4 solutions and AM 350 passivated at 49 °C minutes exposed to (**c**) NaCl and (**d**) H_2SO_4 solutions.

A similar behavior was observed when samples were passivated at 49 °C. In both media, the nitric acid-passivated material performed better. Furthermore, when exposed to H_2SO_4, only the sample that had been passivated in nitric acid for 90 min at 49 °C showed a slope value of passivation (see Table 6).

Recognizing that some values for the two types of corrosion are similar could lead to the development of an additional method for analyzing the slopes alongside the frequencies.

The following formula represents the noise impedance (Z_n), also known as spectral noise resistance.

$$Z_n = \sqrt{\frac{\psi_V(f)}{\psi_I(f)}} \tag{4}$$

Figure 7 shows the noise impedance (Z_n) of the Custom 450 alloy with the different passivated samples. Figure 7a shows the results when exposed to NaCl. The nitric/90 min sample presented the highest Z_n value, 126,654 Ω·cm^2, indicating a higher corrosion resistance. The samples anodized in citric acid presented higher Z_n0 values (see Table 6), indicating a better performance against corrosion than the samples passivated in citric acid. When the samples were exposed to H_2SO_4, the behavior was very similar; the samples passivated in citric acid presented lower corrosion resistance values than those passivated in citric acid.

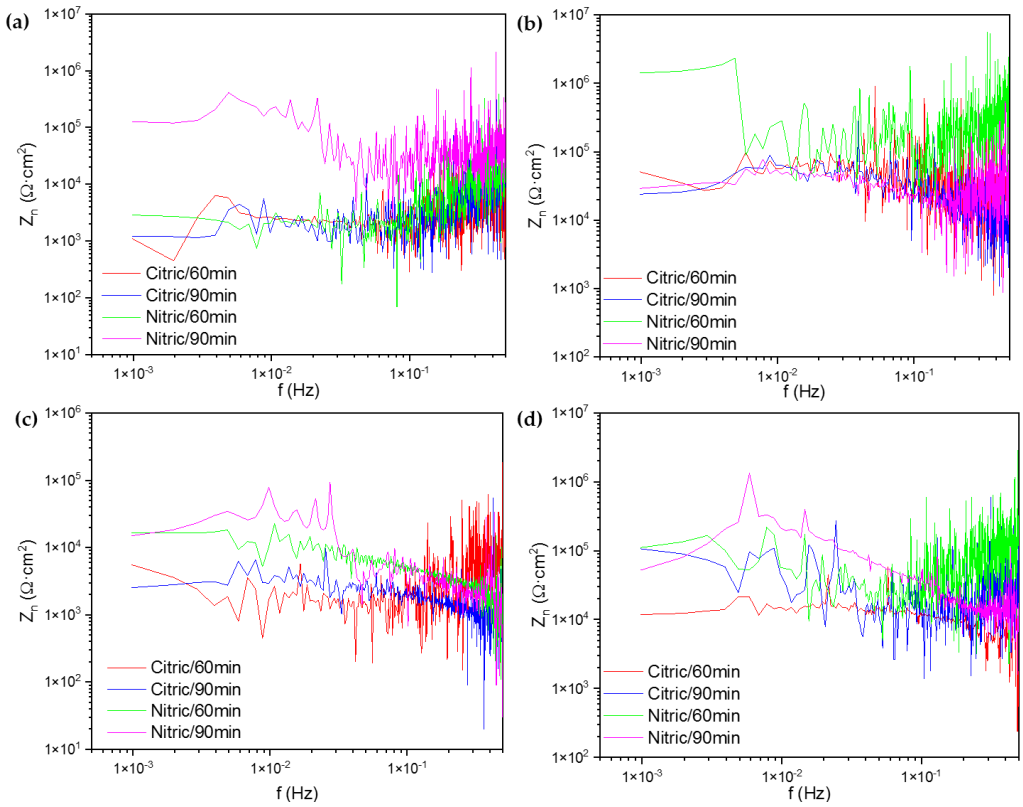

Figure 7. Z_n for Custom 450 passivated at 25 °C exposed to (**a**) NaCl and (**b**) H_2SO_4 solutions and Custom 450 passivated at 49 °C minutes exposed to (**c**) NaCl and (**d**) H_2SO_4 solutions.

Figure 7c shows the behaviors of passivated samples at 49 °C. The samples passivated in nitric acid presented higher Z_n0 values. This behavior was presented in Figure 7d when the samples were exposed to H_2SO_4, meaning there was more corrosion protection when the samples were anodized with nitric acid.

Figure 8 shows the Z_n plots of the passivated AM 350 alloy. Figure 8a shows the behavior when exposed to NaCl; the samples passivated in nitric acid presented the highest resistance, 20,786 and 41,784 Ω·cm^2, for 60 and 90 min, respectively. When the samples were exposed to H_2SO_4, the behavior was similar, indicating that at 25 °C, the samples passivated in nitric acid had a better performance against corrosion.

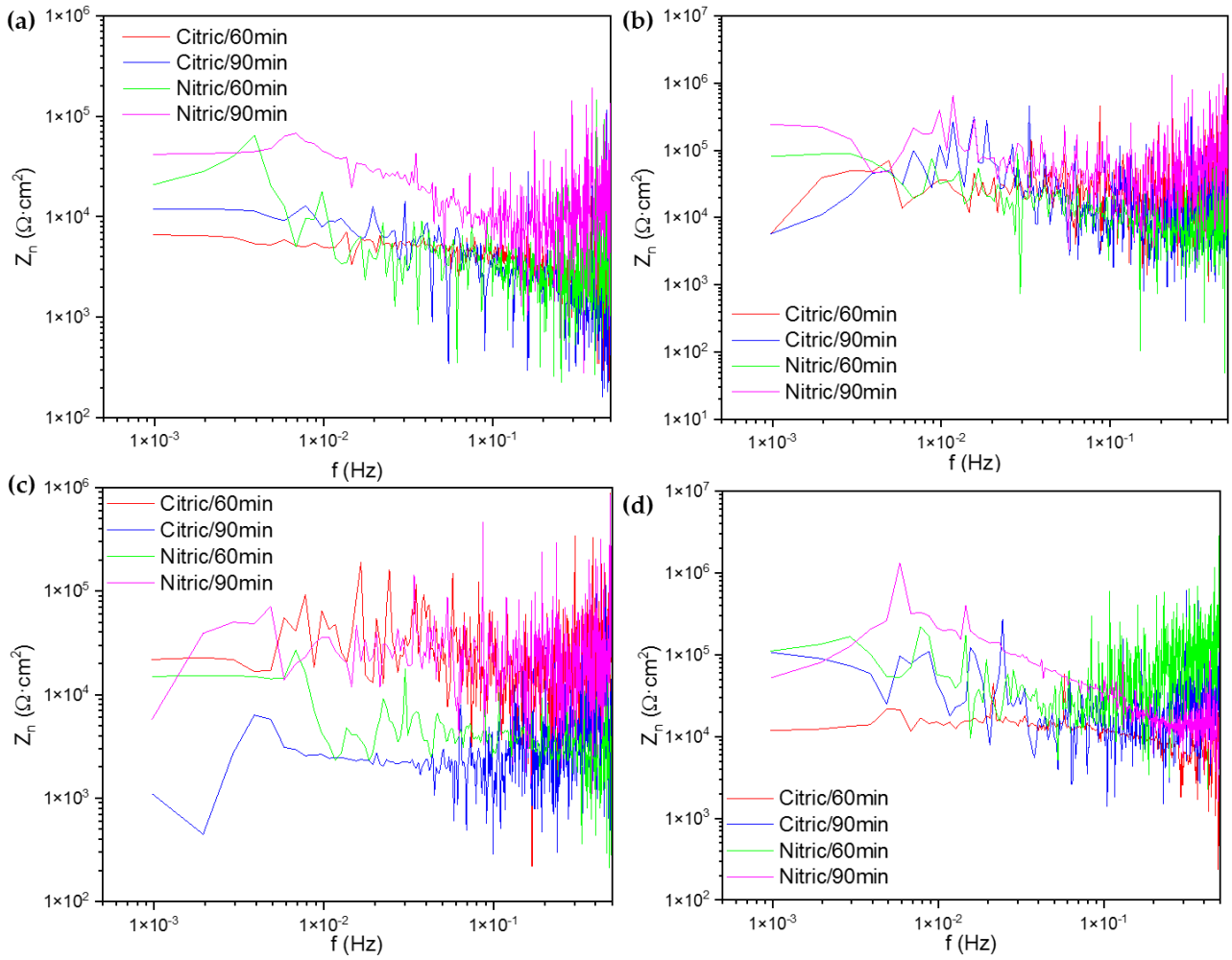

Figure 8. Z_n for AM 350 passivated at 25 °C exposed to (**a**) NaCl and (**b**) H_2SO_4 solutions and AM 350 passivated at 49 °C minutes exposed to (**c**) NaCl and (**d**) H_2SO_4 solutions.

When samples were passivated at 49 °C, the citric/90 min sample showed a lower performance against corrosion, with a Z_n0 value of 5768 Ω·cm^2. The other samples presented similar behaviors with high Z_n0 values (see Table 5). The higher corrosion resistance values of nitric acid-passivated samples are shown in Figure 8d, meaning that the nitric acid passivation produces better results against corrosion.

The HHT is an additional sophisticated technique for identifying the kind and process of corrosion; it assists in eliminating the DC from the original signal [62]. Moreover, this method may also pinpoint the frequency and time at which the energy interchange happens by utilizing an HHT method proposed by Huang et al. [63] in 1998 to study non-stationary signals. The empirical method of decomposition (EMD) is used to calculate this energy and obtain intrinsic functions (IMF), and is referred to as instantaneous energy. The gathered energy can be localized by creating a spectrum with the time–frequency–energy distribution [48]. The proposed EMD by Huang is displayed in Equation (5).

$$x(t) = \sum_{i=1}^{N} h^{(i)}(t) + d(t) \quad (5)$$

The (t) is the average of the time series x(t) trend at a low frequency; it is not decomposable; $h^{(i)}(t)$ is the i-th term of the IMF that is generated; these numbers must meet the requirements that the cross and extreme numbers be equal or different at the maximum and that each point using the local minimum and maximum be zero [63–65]. Equation (6) of HHT is controlled by

$$y_j(t) = \frac{1}{\pi} p \int_{-\infty}^{\infty} \frac{h_j(\tau)}{t-\tau} d\tau \quad (6)$$

The Hilbert transform is denoted by $y_j(t)$, and the IMF is represented by h_j; p is associated with the Cauchy principle and the average of the IMF [63–68].

Figure 9 shows the Hilbert spectra of the Custom 450 alloys passivated at 25 °C. For this figure, only the passivation in nitric acid for 90 min showed a high tendency to present localized corrosion in both media. This occurs because Figure 9g,h shows how the sample presented a high energy accumulation at the middle and high frequencies, indicating that fast corrosion processes occur on the surface. When the alloy was passivated in nitric acid for 60 min and exposed to NaCl (Figure 9e), it presented a high energy accumulation at low frequencies, indicating a uniform process. However, when exposed to H_2SO_4, the sample presented a localized process. This behavior of the localized process for passivated samples exposed to H_2SO_4 is the same for those passivated in citric acid. The passivation in citric acid presented an energy accumulation in the middle and low frequencies, and this happens when the samples presented the diffusion of the localized process, usually related to pitting (see Figure 9a,d).

Figure 10 shows the passivation at 49 °C of the alloy Custom 450. For this temperature, the passivation in citric acid presented a high energy accumulation in the middle and high energy levels in both media, even for 60 and 90 min of passivation. That means the citric acid at this temperature is more susceptible to localized attacks. On the other hand, the samples passivated in nitric acid exposed to NaCl (Figure 10e,g) show a high energy accumulation at low frequencies, indicating a uniform corrosion process on the surface. Additionally, when these samples are exposed to H_2SO_4, they present a high energy accumulation at the high and middle energies, meaning that the samples are susceptible to localized corrosion in this media.

Figure 11 shows the Hilbert spectra of the AM 350 alloys passivated at 25 °C. For this case, all the passivated samples presented an energy accumulation in the middle and high frequencies, meaning that the passivated samples are susceptible to localized corrosion attacks. Only the sample passivated in citric acid for 90 min, Figure 11c, presented some energy accumulation at low frequencies. However, the energy at the middle frequencies indicates a possible pitting diffusion.

Finally, Figure 12 shows the Hilbert spectra of AM 350 alloys passivated at 49 °C. The behavior of this passivation is very similar to the behavior shown in Figure 11. However, Figure 11a–d show the results for passivation in citric acid, and those samples presented a greater energy accumulation at high frequencies. For that reason, the passivated citric acid has a higher trend of presenting localized corrosion.

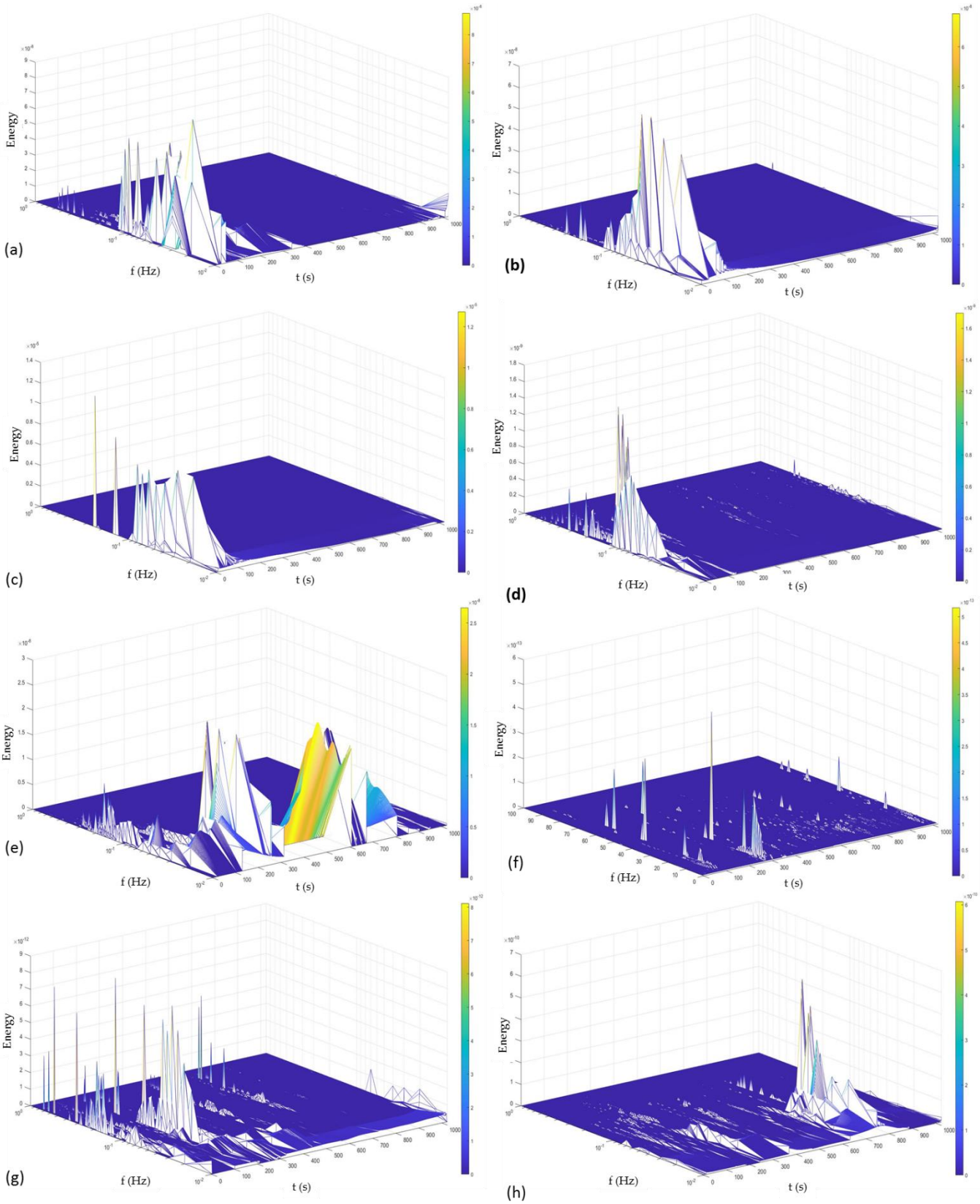

Figure 9. Hilbert spectra for Custom 450 samples passivated at 25 °C in citric acid (**a**–**d**) and nitric acid (**e**–**h**) and exposed to NaCl (**a**,**c**,**e**,**g**) and H_2SO_4 (**b**,**d**,**f**,**h**). (**a**,**b**,**e**,**f**) were passivated for 60 min; (**c**,**d**,**g**,**h**) were passivated for 90 min.

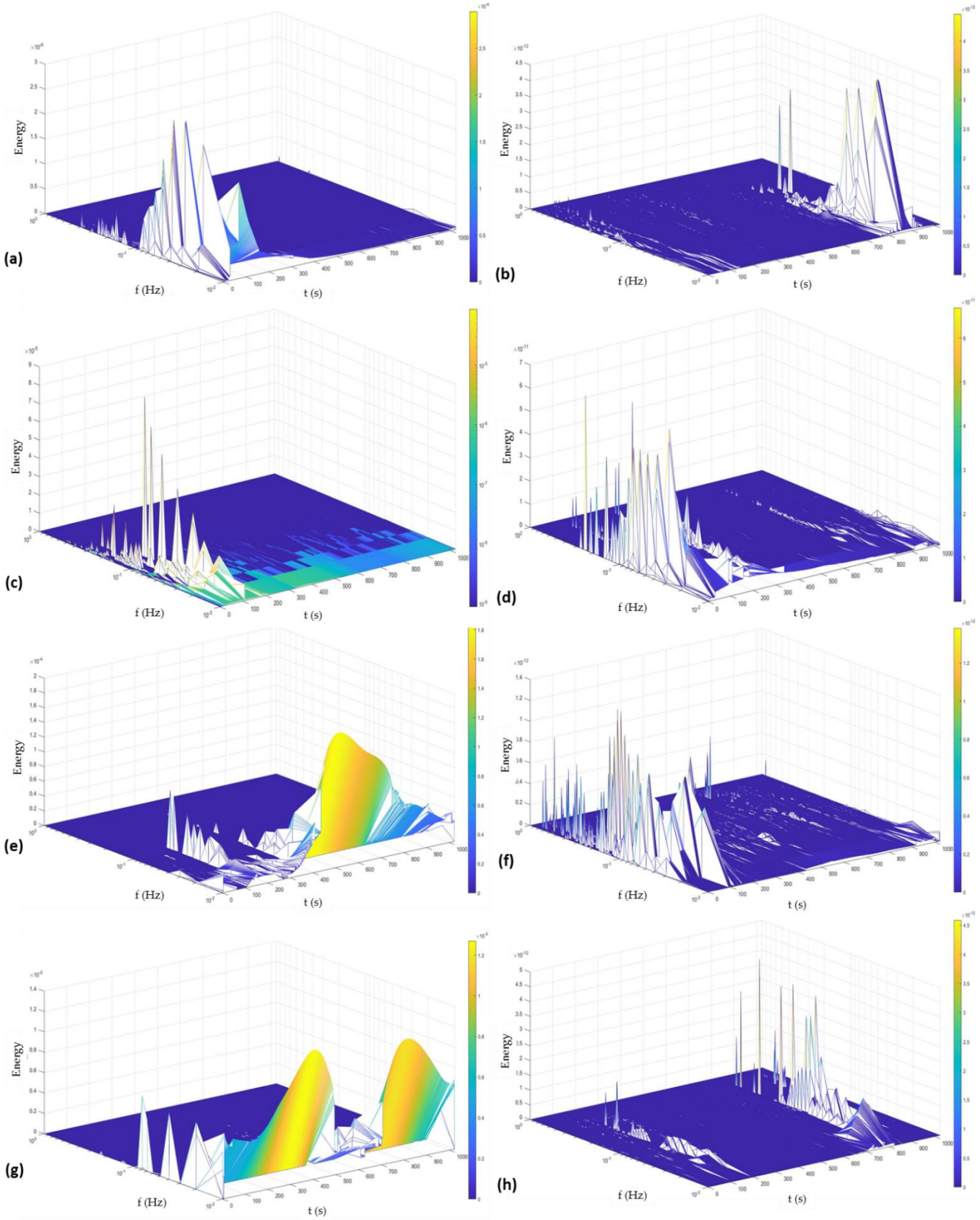

Figure 10. Hilbert spectra for Custom 450 samples passivated at 49 °C in citric acid (**a**–**d**) and nitric acid (**e**–**h**) and exposed to NaCl (**a**,**c**,**e**,**g**) and H_2SO_4 (**b**,**d**,**f**,**h**). (**a**,**b**,**e**,**f**) were passivated for 60 min; (**c**,**d**,**g**,**h**) were passivated for 90 min.

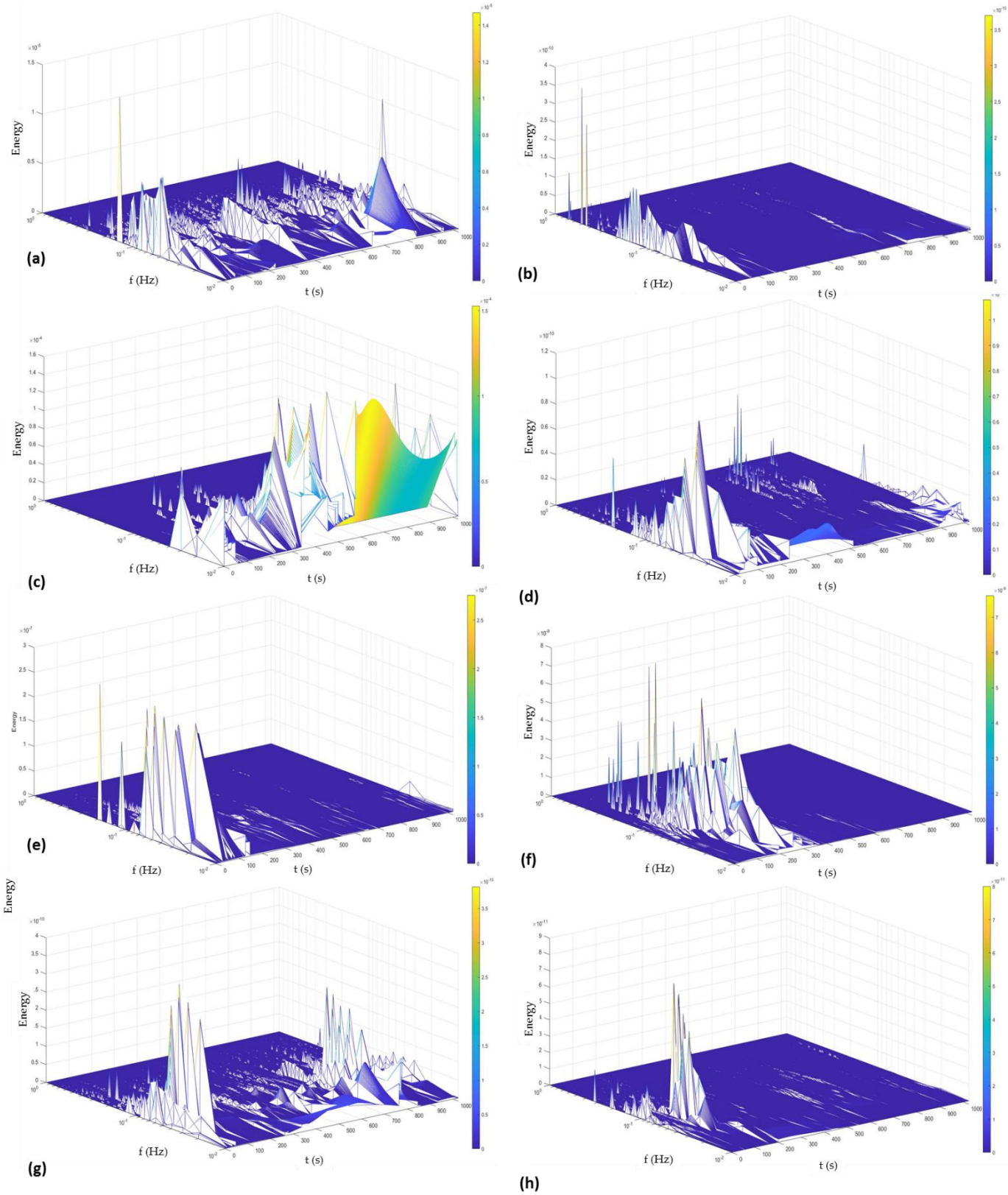

Figure 11. Hilbert spectra for AM 350 samples passivated at 25 °C in citric acid (**a**–**d**) and nitric acid (**e**–**h**) and exposed to NaCl (**a**,**c**,**e**,**g**) and H_2SO_4 (**b**,**d**,**f**,**h**). (**a**,**b**,**e**,**f**) were passivated for 60 min; (**c**,**d**,**g**,**h**) were passivated for 90 min.

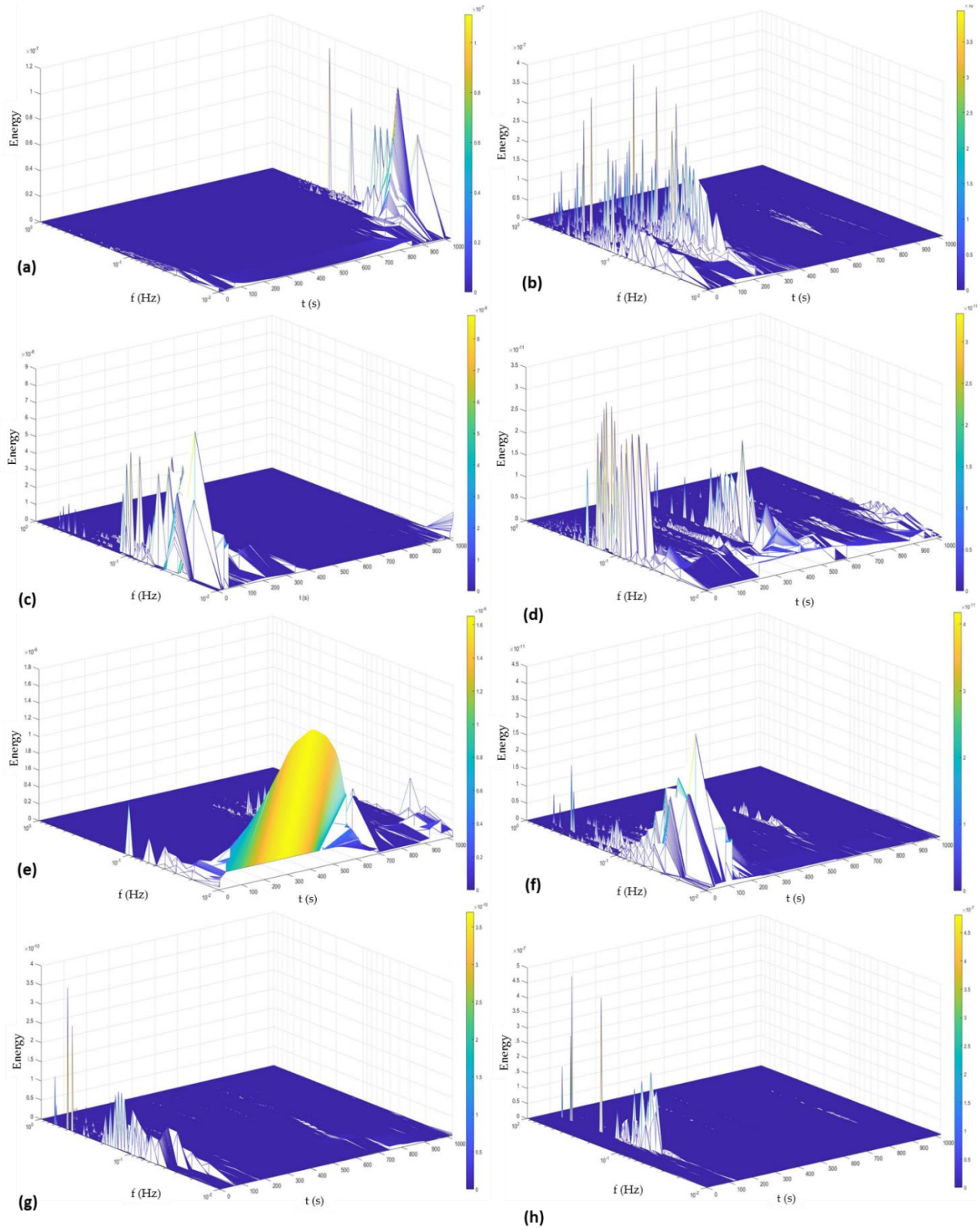

Figure 12. Hilber spectra for AM 350 samples passivated at 49 °C in citric acid (**a**–**d**) and nitric acid (**e**–**h**) and exposed to NaCl (**a**,**c**,**e**,**g**) and H_2SO_4 (**b**,**d**,**f**,**h**). (**a**,**b**,**e**,**f**) were passivated 60 min; (**c**,**d**,**g**,**h**) were passivated 90 min.

4. Discussion

The PHSSs' potentiodynamic polarization curves (Figures 3 and 4) have distinct forms, indicating that there is passivation in the anodic reaction, but there is a difference in their pitting potentials due to the various electrochemical processes in the test solutions of NaCl and H_2SO_4. However, the potentiodynamic polarization curves exhibit two distinctive causes. When the PHSS is immersed in the H_2SO_4 solution, a passivation layer forms on the surface of the Cr–Fe alloy, determining its corrosion resistance and triggering this passivation protection mechanism. Chromium oxides play a key role in passive films, and the OH^- anodic interactions cause this behavior. The PHSS sample's elevated current density is the cause of transpassivation and secondary passivation. A stable passivation film is represented by a pseudo-passivation when the samples are submerged in a NaCl solution. This defense mechanism creates a passive layer of Cr-rich oxides and oxyhydroxides that stops oxygen from penetrating the interior layer and shields the base material from corrosive ions, like the Cl^- to which the samples were exposed [69–76].

According to Gaona et al. [37], when samples are submerged in a NaCl solution, an unstable passivation film causes an increase in the current density, affecting the corrosion kinetics of stainless steel. On the other hand, austenitic stainless steels submerged in a H_2SO_4 solution displayed transients linked to secondary passivation—the regeneration of the passive layer—and transpassivation, or the rupture of the passivation film.

The results obtained using the EN (electrochemical noise) technique showed that the alloys passivated in citric acid have a high susceptibility to pitting attacks and present less corrosion resistance. The PHSS Custom 450 passivated in nitric acid at 25 °C for 60 min presented the lowest Ψ^0 (−130 dBi), indicating that the energy transference and kinetics will be slower than in the other alloys. This occurs when exposed to H_2SO_4. Also, that sample presented a higher noise impedance of 1,410,107 $\Omega \cdot cm^2$. The best performance against corrosion in NaCl was of Custom 450 passivated in nitric acid at 25 °C for 90 min, with 126,654 $\Omega \cdot cm^2$. These results indicate that the PHSS with a martensitic phase has a better predisposition to generate a stable oxide layer. Also, the development of that oxide layer is better when the passivation temperature is 25 °C in nitric acid. However, all these samples present localized corrosion.

Also, the corrosion rate analysis showed that the passivated Custom 450 presented lower corrosion rates with values of $\times 10^{-4}$ mm/yr order when exposed to NaCl, meaning that the passivated samples exposed to H_2SO_4 presented higher corrosion rates with value orders of $\times 10^{-2}$. However, the best performance occurs with the samples passivated in nitric acid.

PHSSs passivated in both acids demonstrated a trend of pitting corrosion. However, the passivation in nitric acid presented a greater energy accumulation at the middle and high frequencies, indicating localized corrosion. In the research of Lara et al., Samaniego et al., and Gaydos et al. [7,14,15,77,78], it was concluded that nitric acid raises the passive layer's chromium content, clearing MnS inclusions from the surface and raising the likelihood of individual pitting. Because of the presence of MnS, the samples passivated in nitric acid in this study showed higher corrosion than those passivated in citric acid. Alterations in the acid content or alternative solutions like citric acid, where the pitting process was more regulated, should be employed to decrease the amount of MnS. In Equations (7) and (8), we show that the processes above can remove MnS, and the acid content may impact the passivation stability.

$$MnS + 2H^+ \rightarrow Mn^{2+} + H_2S \tag{7}$$

$$2MnS + 3H_2O \rightarrow 2Mn^{2+} + S_2O_3^{2-} + 6H^+ + 8e^- \tag{8}$$

It is important to mention that the higher passivation range values are from the samples passivated in nitric acid, even for Custom 450 and AM 350. However, the AM 350 alloy presented a higher passivation range when exposed to NaCl. Meanwhile, the Custom 450 alloy presented a higher passivation range in H_2SO_4. The lower values in the

passivation range of citric acid indicate that the passive layer generated by this electrolyte is weak compared to the one generated by nitric acid. This behavior was also shown when the samples were evaluated using EN, where a better performance against corrosion was obtained with nitric acid passivation, indicating a more effective passive layer.

Some publications [79–81] claim that the data showed a somewhat consistent range in the passive potentials of PHSSs during passivation. It generates a relatively stable passive film, since the passive current density is the same. Nevertheless, the electrochemical process of the anodic reaction is still underway. The passive film is unstable in that instance, and the passive current density differs. The HHT analysis reveals this unstable passive layer, with the samples exhibiting localized corrosion preponderance. This outcome confirms the findings of Samaniego et al. [15], who reported localized corrosion in the samples passivated in nitric acid. In contrast to the nitric acid-passivated PHSS, the citric acid-passivated PHSS showed a greater tendency toward localized corrosion.

Some writers say stainless steels exhibit passive films before and after transformation [82–86]. With noble electrode potentials, transpassivation is a dissolving mechanism in which the steel is activated and starts to dissolve [21,87], and the anodic branch experiences passivation (a feature of stainless steel that has been passivated). Most research has concentrated on this area, ignoring that, as this study found, some acid solutions can form a second layer for passivation.

Iron oxide and chromium oxide coatings, frequently found in PHSSs, are formed in the passive zone [32,88,89]. Consequently, the chromium trihydroxide compound $Cr(OH)_3$ is developed due to the selective dissolution of Cr^{3+} on the surfaces of stainless steels (see Equation (9)). When $Cr(OH)_3$ is present on the surface, the hydroxides react to generate a continuous passive layer of chromium oxide Cr_2O_3 (see Equation (10)) [16,90,91].

$$Cr^{3+} + 3OH^- \rightarrow Cr(OH)_3 + 3e^- \tag{9}$$

$$Cr(OH)_3 + Cr + 3OH^- \rightarrow Cr_2O_3 + 3H_2O + 3e^- \tag{10}$$

As previously indicated, iron and chromium oxidation are the primary sources of anodic reactions during the passivation film growth period. Equations (11)–(13) [92–94] show the iron oxidation reactions:

$$3Fe + 8OH^- \rightarrow Fe_3O_4 + 4H_2O + 8e^- \tag{11}$$

$$2Fe_3O_4 + 2OH^- + 2H_2O \rightarrow 6FeOOH + 2e^- \tag{12}$$

$$2Fe_3O_4 + 2OH^- \rightarrow 3Fe_2O_3 + H_2O + 2e^- \tag{13}$$

In the passivated PHSS samples submerged in a 5% NaCl solution, pseudo-passivation occurred. The passive films generated on the PHSS may be in an incomplete steady state, because the current density increases with increases in the anodic potential rather than reaching the stable state within the passive zone. This instability is brought on by chloride ions (Cl^-), which have a strong affinity for steel surfaces and can diffuse into the steel through holes in the passive surface film. This reduces the efficiency of the PHSS's passive film [7,16,95,96]. The creation of the $Cr(OH)_3$ film may be linked to the pseudo-passivation phenomenon seen in the polarization curves of several passivated samples. The separation of the $Cr(OH)_3$ film occurs simultaneously with the rupture of the pseudo-passivated region. Because of this, the $Cr(OH)_3$ film performs the role of a pseudo-passive film [97–99]. According to certain studies, $Cr(OH)_3$ may inhibit the iron's dissolution process, isolate the corrosive media, and decrease the number of active sites in the iron dissolution process [100–103]. According to the literature [14,16,104–109], citric acid can be an ecological alternative to replace nitric acid, since citric acid passivation indicates similar results to the nitric acid solution. In future works, it is necessary to improve an increase the passivation time of citric acid electrolytes due to the properties of this electrolyte. Citric acid is weaker than nitric acid.

The protection mechanism (see Figure 13a) occurs due to the formation of a passive layer formed by oxides and oxy/hydroxides rich in Cr that prevent the propagation of oxygen to the internal layer and protect the base material from the penetration of corrosive ions, such as the Cl^- in which the samples were exposed. In the case of Figure 13b, the protection mechanism is different since passivation occurs. The passivation film formed on the surface of the Cr–Fe alloy determines its corrosion resistance. Chromium oxides are essential in passive films [110–112].

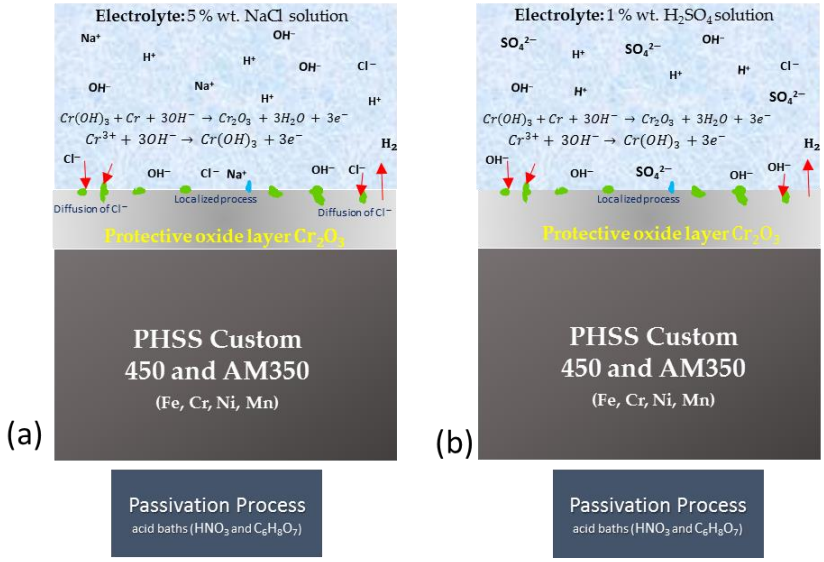

Figure 13. Model diagrams of passivation processes in citric and nitric acid baths for CUSTOM 450 and AM 350 stainless steels exposed to (**a**) 5 wt.% NaCl solution and (**b**) 1 wt.% H_2SO_4 solution.

5. Conclusions

The conclusions are as follows:

- The AM 350 stainless steel had austenite (γ) and delta (δ) ferrite phases, while the Custom 450 stainless steel displayed a martensitic (α′) phase, respectively.
- The results indicate that the corrosion current densities of H_2SO_4 were measured to be between 10^{-2} and 10^{-3} mA/cm^2, whereas the Custom and AM 350 steels passivated in solutions of nitric and citric acid presented corrosion current densities of 10^{-4} mA/cm^2.
- The PHSS samples passivated in nitric acid and immersed in sodium chloride have higher pitting potentials than the samples passivated in citric acid.
- Using the bath of citric acid in the place of nitric acid during the passivation process creates a system in which the electrochemical behavior is similar, mixed by activation, and where the anodic branch presents a series of events such as pseudo-passivation and/or passivation–transpassivation–secondary passivation.
- The EN results show that the PHSSs passivated in nitric acid obtained higher values of noise impedance, indicating a higher corrosion resistance than the samples passivated in citric acid.
- The PHSSs passivated in nitric acid presented a higher corrosion resistance, indicating that it is still the better option to passivate PHSS. This can be observed in the corrosion resistance by the corrosion rates of PPCs and the noise impedance results.
- The HHT analysis shows that the nitric acid-passivated PHSS presented a high energy accumulation at the middle and high frequencies, indicating susceptibility to a localized attack.
- The Z_n analyses show that Custom 450 passivated in nitric acid had more impedance noise in H_2SO_4 (1,410,107 Ω·cm^2) when it was passivated at 25 °C for 60 min. Also,

the same PHSS passivated in the same electrolyte for 90 min presented the highest noise impedance, 126,654 $\Omega \cdot cm^2$, when exposed to NaCl.

Author Contributions: Conceptualization, F.A.-C., M.V.-T. and C.G.-T.; methodology, M.V.-T., E.M.-B., M.L.-B., J.M.J.-M., F.E.-L. and G.S.-H.; data curation, F.A.-C., L.D.L.-L., D.N.-M., F.A.-C., G.S.-H., M.A.B.-Z. and F.E.-L.; formal analysis, F.A.-C., E.M.-B., M.A.B.-Z., L.D.L.-L., D.N.-M., M.L.-B. and C.G.-T.; writing—review and editing, F.A.-C., M.V.-T., J.M.J.-M. and C.G.-T. All authors have read and agreed to the published version of the manuscript.

Funding: This research received no external funding.

Data Availability Statement: The data presented in this study are available on request from the corresponding author (privacy).

Acknowledgments: The authors would like to thank the UANL-CA-316 working group and Universidad Autónoma de Nuevo León (UANL) for the facilities provided to perform this investigation.

Conflicts of Interest: The authors declare no conflicts of interest.

References

1. Martinez, B.; Tiburcio, C.G.; Bastidas, D.; Lara-Banda, M.; Samaniego, O.; Calderon, F.A. Electrochemical Evaluation of 15-5PH Stainless Steel Passivated in Citric Acid. *ECS Trans.* **2022**, *106*, 223. [CrossRef]
2. Martínez-Aparicio, B.; Martínez-Bastidas, D.; Gaona-Tiburcio, C.; Martin, U.; Cabral-Miramontes, J.; Almeraya-Calderón, F. Localized corrosion of 15–5 PH and 17–4 PH stainless steel in NaCl solution. *J. Solid State Electrochem.* **2023**, *27*, 2993–3001. [CrossRef]
3. Gloria, A.; Montanari, R.; Richetta, M.; Varone, A. Alloys for aeronautic applications: State of the art and perspectives. *Metals* **2019**, *9*, 662. [CrossRef]
4. Mouritz, P.A. *Introduction to Aerospace Materials*; Woodhead Publishing: Cambridge, UK, 2012.
5. Lopes, J.C. Material selection for aeronautical structural application. *Sci. Technol. Adv. Mater.* **2008**, *20*, 78–82.
6. Lo, K.H.; Shek, C.H.; Lai, J.K.L. Recent developments in stainless steels. *Mat. Sci. Eng. R.* **2009**, *65*, 39–104. [CrossRef]
7. Lara Banda, M.; Gaona-Tiburcio, C.; Zambrano-Robledo, P.; Cabral, M.J.A.; Estupinan, F.; Baltazar-Zamora, M.A.; Almeraya-Calderon, F. Corrosion Behaviour of 304 Austenitic, 15–5PH and 17-4PH Passive Stainless Steels in acid solutions. *Int. J. Electrochem. Sci.* **2018**, *13*, 10314–10324. [CrossRef]
8. Gialanella, S.; Malandruccolo, A. *Aerospace Alloys*; Topics in Mining, Metallurgy and Materials Engineering; Springer: Cham, Switzerland, 2020; ISSN 2364-3307. [CrossRef]
9. Cobb, H.M. *The History of Stainless Steel*; ASM International: Cleveland, OH, USA, 2010; pp. 189–192.
10. Ha, H.Y.; Jang, J.H.; Lee, T.H.; Won, C.; Lee, C.H.; Moon, J.; Lee, C.G. Investigation of the localized corrosion and passive behavior of type 304 stainless steels with 0.2–1.8 wt% B. *Materials* **2018**, *11*, 2097. [CrossRef]
11. Schmuki, P. From bacon to barriers: A review on the passivity of metal and alloys. *J. Solid State Electr.* **2002**, *6*, 145–164. [CrossRef]
12. Dong, H.; Esfandiari, M.; Li, X.Y. On the microstructure and phase identification of plasma nitrided 17-4PH precipitation hardening stainless steel. *Surf. Coat. Technol.* **2008**, *202*, 2969–2975. [CrossRef]
13. Hsiao, C.N.; Chiou, C.S.; Yang, J.R. Aging reactions in a 17-4 PH stainless steel. *Mater. Chem. Phys.* **2002**, *74*, 134–142. [CrossRef]
14. Gaydos, S.P. Passivation of aerospace stainless parts with citric acid solutions. *Plat. Surf. Finish.* **2003**, *90*, 20–25.
15. Samaniego-Gámez, O.; Almeraya-Calderón, F.; Chacón-Nava, J.; Maldonado-Bandala, E.; Nieves-Mendoza, D.; Flores-De los Rios, J.P.; Gaona-Tiburcio, C. Corrosion Behavior of Passivated CUSTOM450 and AM350 Stainless Steels for Aeronautical Applications. *Metals* **2022**, *12*, 666. [CrossRef]
16. Almeraya-Calderón, F.; Estupiñán, F.; Zambrano, R.P.; Martínez-Villafañe, A.; Borunda, T.A.; Colás, O.R.; Gaona-Tiburcio, C. Análisis de los transitorios de ruido electroquímico para aceros inoxidables 316 y-DUPLEX 2205 en NaCl y FeCl. *Rev. Metal.* **2012**, *4*, 147–156. [CrossRef]
17. Mehdipour, M.; Naderi, R.; Markhali, B.P. Electrochemical study of effect of the concentration of azole derivatives on corrosion behavior of stainless steel in H_2SO_4. *Prog. Org. Coat.* **2014**, *77*, 1761–1767. [CrossRef]
18. Kelly, R.G.; Scully, J.R.; Shoesmith, D.W.; Buchheit, G. *Electrochemical Techniques in Corrosion Science and Engineering*; Taylor & Francis: Boca Raton, FL, USA, 2002; pp. 54–123.
19. Kearns, J.R.; Eden, D.A.; Yaffe, M.R.; Fahey, J.V.; Reichert, D.L.; Silverman, D.C. ASTM Standardization of Electrochemical Noise Measurement. In *Electrochemical Noise Measurement for Corrosion Applications*; Kearns, J.R., Scully, J.R., Roberge, P.R., Reirchert, D.L., Dawson, L., Eds.; ASTM International: Materials Park, OH, USA, 1996; pp. 446–471.
20. Botana, P.J.; Bárcena, M.M.; Villero, Á.A. *Ruido Electroquímico: Métodos de Análisis*; Septem Ediciones: Cadiz, Spain, 2002; pp. 50–70.
21. Gaona-Tiburcio, C.; Aguilar, L.M.R.; Zambrano-Robledo, P.; Estupiñán-López, F.; Cabral-Miramontes, J.A.; Nie-ves-Mendoza, D.; Castillo-González, E.; Almeraya-Calderón, F. Electrochemical Noise Analysis of Nickel Based Superalloys in Acid Solutions. *Int. J. Electrochem. Sci.* **2014**, *9*, 523–533. [CrossRef]

22. Lara-Banda, M.; Gaona-Tiburcio, C.; Zambrano-Robledo, P.; Delgado-E, M.; Cabral-Miramontes, J.A.; Nieves-Mendoza, D.; Maldonado-Bandala, E.; Estupiñan-López, F.; Chacón-Nava, J.G.; Almeraya-Calderón, F. Alternative to nitric acid passivation of 15-5 and 17-4PH stainless steel using electrochemical techniques. *Materials* **2020**, *13*, 2836. [CrossRef] [PubMed]
23. Bragaglia, M.; Cherubini, V.; Cacciotti, I.; Rinaldi, M.; Mori, S.; Soltani, P.; Nanni, F.; Kaciulis, S.; Montesperelli, G. Citric Acid Aerospace Stainless Steel Passivation: A Green Approach. In Proceedings of the CEAS Aerospace Europe Conference 2015, Delft, The Netherlands, 7–11 September 2015.
24. Marcelin, S.; Pébèrea, N.; Régnierb, S. Electrochemical characterisation of a martensitic stainless steel in a neutral chloride solution. *Electrochim. Acta* **2013**, *87*, 32–40. [CrossRef]
25. Lin, C.K.; Chu, C.C. Mean stress effects on low-cycle fatigue for a precipitation-hardening martensitic stainless steel in different tempers. *Fatigue Fract. Eng. Mater. Struct.* **2000**, *23*, 545–553. [CrossRef]
26. Nagiub, A.M. Electrochemical Noise Analysis for Different Green Corrosion Inhibitors for Copper Exposed to Chloride Media. *Port. Electrochim. Acta* **2017**, *35*, 201–210. [CrossRef]
27. Nakasa, K.; Satoh, H. The effect of hydrogen-charging on the fatigue crack propagation behavior of β-titanium alloys. *Corros. Sci.* **1996**, *38*, 457–468. [CrossRef]
28. Dawson, D.L. Electrochemical Noise Measurement: The definitive In-Situ Technique for Corrosion Applications? In *Electrochemical Noise Measurement for Corrosion Applications STP 1277*; Kearns, J.R., Scully, J.R., Roberge, P.R., Reirchert, D.L., Dawson, L., Eds.; ASTM International: Materials Park, OH, USA, 1996; pp. 3–39.
29. Cottis, R.; Turgoose, S.; Mendoza-Flores, J. The Effects of Solution Resistance on Electrochemical Noise Resistance Measurements: A Theorical Analysis. In *Electrochemical Noise Measurement for Corrosion Applications STP 1277*; Kearns, J.R., Scully, J.R., Roberge, P.R., Reirchert, D.L., Dawson, L., Eds.; ASTM International: Materials Park, OH, USA, 1996; pp. 93–100.
30. Brockwell, P.J.; Davis, R.A. *Introduction to Time Series and Forecasting*, 3rd ed.; Springer: Zürich, Switzerland, 2002; pp. 1–68.
31. Homborg, A.M.; Tinga, T.; Zhang, X.; Van Westing, E.P.M.; Ferrari, G.M.; Wit, J.H.W.; Mol, J.M.W. A Critical Appraisal of the Interpretation of Electrochemical Noise for Corrosion Studies. *Corrosion* **2017**, *70*, 971–987. [CrossRef] [PubMed]
32. El-Taib Heakal, F.; Ameer, M.A.; El-Aziz, A.M.; Fekry, A.M. Electrochemical behavior of Mo-containing austenitic stainless steel in buffer solutions. *Mat. Werkstofftech.* **2004**, *35*, 407–413. [CrossRef]
33. El-Taib Heakal, F.; Ghoneim, A.; Fekry, A. Stability of spontaneous passive films on high strength Mo-containing stainless steels in aqueous solutions. *J. Appl. Electrochem.* **2007**, *37*, 405–413. [CrossRef]
34. Ameer, M.A.; Fekry, A.M.; El-TaibHeakal, F. Electrochemical behaviour of passive films on molybdenum-containing austenitic stainless steels in aqueous solutions. *Electrochim. Acta* **2007**, *50*, 43–49. [CrossRef]
35. Mollapour, Y.; Poursaeidi, E. Experimental and numerical analysis of Pitting Corrosion in CUSTOM 450 Stainless Steel. *Eng. Fail. Anal.* **2021**, *128*, 105589. [CrossRef]
36. Samaniego-Gámez, O.; Almeraya-Calderón, F.; Maldonado-Bandala, E.; Nieves-Mendoza, D.; Olguín-Coca, J.; Jáquez-Muñoz, J.M.; Cabral-Miramontes, J.; Flores-De los Rios, J.P.; Bautista-Margulis, R.G.; Gaona-Tiburcio, C. Corrosion Behavior of Passivated Martensitic and Semi-Austenitic Precipitation Hardening Stainless Steel. *Metals* **2022**, *12*, 1033. [CrossRef]
37. Gaona Tiburcio, C.; Samaniego-Gámez, O.; Jáquez-Muñoz, J.; Baltazar-Zamora, M.A.; Landa-Ruiz, L.; Lira-Martínez, A.; Flores-De los Rios, J.P.; Cabral-Miramontes, J.; Estupinán-López, F.; Almeraya-Calderon, F. Frequency-Time Domain Analysis of Electrochemical Noise of Passivated AM350 Stainless Steel for Aeronautical Applications. *Int. J. Electrochem. Sci.* **2022**, *17*, 220950. [CrossRef]
38. Villegas-Tovar, J.; Gaona-Tiburcio, C.; Lara-Banda, M.; Maldonado-Bandala, E.; Baltazar-Zamora, M.A.; Cabral-Miramontes, J.; Nieves-Mendoza, D.; Olguin-Coca, J.; Estupiñan-Lopez, F.; Almeraya-Calderón, F. Electrochemical Corrosion Behavior of Passivated Precipitation Hardening Stainless Steels for Aerospace Applications. *Metals* **2023**, *13*, 835. [CrossRef]
39. AM 350 Technical Data. Available online: https://www.hightempmetals.com/techdata/hitempAM350data.php (accessed on 29 September 2022).
40. Custom 450® Stainless Steel. Available online: https://www.ulbrich.com/uploads/data-sheets/Custom-450-Stainless-Steel-Wire-UNS-S45000.pdf (accessed on 31 April 2022).
41. *ASTM A380-17*; Standard Practice for Cleaning, Descaling and Passivation of Stainless-Steel Parts, Equipment, and Systems. ASTM International: West Conshohocken, PA, USA, 1999.
42. *ASTM E3-95*; Standard Practice for Preparation of Metallographic Specimens. ASTM International: West Conshohocken, PA, USA, 1995.
43. *SAE AMS 2700F*; Passivation of Corrosion Resistant Steels. Aerospace Material Specification. SAE International: Warrendale, PA, USA, 2018.
44. *ASTM A967-17*; Standard Specification for Chemical Passivation Treatments for Stainless Steel Parts. ASTM International: West Conshohocken, PA, USA, 1999.
45. *ASTM G5-11*; Standard Reference Test Method for Making Potentiostatic and Potentiodynamic Anodic Polarization Measurements. ASTM International: West Conshohocken, PA, USA, 2011.
46. Jaquez-Muñoz, J.; Gaona-Tiburcio, C.; Lira-Martinez, A.; Zambrano-Robledo, P.; Maldonado-Bandala, E.; Samaniego-Gamez, O.; Nieves-Mendoza, D.; Olguin-Coca, J.; Estupiñan-Lopez, F.; Almeraya-Calderon, F. Susceptibility to pitting corrosion of Ti-CP2, Ti-6Al-2Sn-4Zr-2Mo, and Ti-6Al-4V alloys for aeronautical applications. *Metals* **2021**, *11*, 1002. [CrossRef]

47. Zhang, Z.; Zhao, Z.; Bai, P.; Li, X.; Liu, B.; Tan, J.; Wu, X. In-Situ Monitoring of Pitting Corrosion of AZ31 Magnesium Alloy by Combining Electrochemical Noise and Acoustic Emission Techniques. *J. Alloys Compd.* **2021**, *878*, 160334. [CrossRef]
48. *ASTM G199-09*; Standard Guide for Electrochemical Noise Measurement. ASTM International: West Conshohocken, PA, USA, 2020.
49. Galvan-Martinez, R.; Orozco-Cruz, R.; Torres-Sanchez, R.; Martinez, E.A. Corrosion Study of the X52 Steel Immersed in Seawater with a Corrosion Inhibitor Using a Rotating Cylinder Electrode. *Mater. Corros.* **2010**, *61*, 872–876. [CrossRef]
50. Jáquez-Muñoz, J.M.; Gaona-Tiburcio, C.; Méndez-Ramírez, C.T.; Baltazar-Zamora, M.Á.; Estupinán-López, F.; Bautista-Margulis, R.G.; Cuevas-Rodríguez, J.; Flores-De los Rios, J.P.; Almeraya-Calderón, F. Corrosion of Titanium Alloys Anodized Using Electrochemical Techniques. *Metals* **2023**, *13*, 476. [CrossRef]
51. Tafel, J. Über die Polarisation bei kathodischer Wasserstoffentwicklung. *Z. Phys. Chem.* **1905**, *50*, 641–712. [CrossRef]
52. Butler, J.A.V. Studies in heterogeneous equilibria. Part II.—The kinetic interpretation on the Nernst theory of electromotive force. *Trans. Faraday Soc.* **1924**, *19*, 729–733. [CrossRef]
53. Bojinov, M.; Fabricius, G.; Laitinen, T.; Saario, T. The mechanism of the transpassive dissolution of chromium in acidic sulfate solutions. *J. Electrochem. Soc.* **1998**, *145*, 2043–2050. [CrossRef]
54. Cottis, R. Interpretation of Electrochemical Noise Data. *Corrosion* **2001**, *57*, 265–285. [CrossRef]
55. Eden, D.A. Electrochemical Noise—The First Two Octaves. In Proceedings of the Corrosion/98, San Diego, CA, USA, 22–27 March 1998; Paper 386, Volume 1, pp. 1–31.
56. Coakley, J.; Vorontsov, V.A.; Littlell, K.C.; Heenan, R.K.; Ohnuma, G.; Jones, N.G.; Dye, D. Nanoprecipitation in a beta-titanium alloy. *J. Alloys Compd.* **2015**, *623*, 146. [CrossRef]
57. Bertocci, U.; Huet, F. Noise Analysis Applied to Electrochemical Systems. *Corrosion* **1995**, *51*, 131–144. [CrossRef]
58. Lee, C.C.; Mansfeld, F. Analysis of electrochemical noise data for a passive system in the frequency domain. *Corr. Sci.* **1998**, *40*, 959–962. [CrossRef]
59. Legat, A.; Dolecek, V. Corrosion Monitoring System Based on Measurement and Analysis of electrochemical Noise. *Corrosion* **1995**, *51*, 295–300. [CrossRef]
60. Homborg, A.M.; Cottis, R.A.; Mol, J.M.C. An integrated approach in the time, frequency and time-frequency domain for the identification of corrosion using electrochemical noise. *Electrochim. Acta* **2016**, *222*, 627–640. [CrossRef]
61. Martinez-Villafane, A.; Chacon-Nava, J.G.; Gaona-Tiburcio, C.; Almeraya-Calderon, F.; Dominguez-Patino, G.; Gonzalez-Rodriguez, J.G. Oxidation performance of a Fe–13Cr alloy with additions of rare earth elements. *Mater. Sci. Eng. A* **2003**, *363*, 15–19. [CrossRef]
62. Esfandiari, M.; Dong, H. The corrosion and corrosion–wear behaviour of plasma nitrided 17-4PH precipitation hardening stainless steel. *Surf. Coat. Technol.* **2007**, *202*, 466–478. [CrossRef]
63. Huang, N.E.; Shen, Z.; Long, Z.R.; Wu, M.C.; Shih, H.H.; Zheng, Q.; Yen, N.C.; Tung, C.C.; Liu, H.H. The empirical mode decomposition and the Hilbert spectrum for nonlinear and non-stationary time series analysis. *Proc. R. Soc. Lond.* **1998**, *454*, 903–995. [CrossRef]
64. Cabral-Miramontes, J.A.; Gaona-Tiburcio, C.; Almeraya-Calderón, F.; Estupiñan-Lopez, H.F.; Pedraza-Basulto, G.; Poblano-Salas, C. Parameter Studies on High-Velocity Oxy-Fuel Spraying of CoNiCrAlY Coatings Used in the Aeronautical Industry. *Int. J. Corros.* **2014**, 1–8. [CrossRef]
65. Cheng, M.; Chaofang, D.; Zhongyu, C.; Kui, X. A comparative study of primary and secondary passive films formed on AM355 stainless steel in 0.1 M NaOH. *Appl. Surf. Sci.* **2018**, *427*, 763–773. [CrossRef]
66. Zhao, B.; Li, J.H.; Hu, R.G.; Du, R.G.; Lin, C.J. Study on the corrosion behavior of reinforcing steel in cement mortar by electrochemical noise measurements. *Electrochim. Acta* **2007**, *52*, 3976–3984. [CrossRef]
67. Xia, D.; Shi, S.; Behnamian, Y.; Hu, W.; Cheng, Y.F.; Luo, J.; Huet, F. Review—Electrochemical Noise Applied in Corrosion Science: Theoretical and Mathematical Models towards Quantitative Analysis. *J. Electrochem. Soc.* **2020**, *167*, 081507. [CrossRef]
68. Li, L.; Qiao, Y.; Zhang, L.; Ma, A.; Ma, R.; Zheng, Y. Understanding the Corrosion Behavior of Nickel–Aluminum Bronze Induced by Cavitation Corrosion Using Electrochemical Noise: Selective Phase Corrosion and Uniform Corrosion. *Materials* **2023**, *16*, 669. [CrossRef]
69. Rivera-Cerezo, H.; Gaona-Tiburcio, C.; Cabral-Miramontes, J.; Bautista-Margulis, R.G.; Nieves-Mendoza, D.; Maldonado-Bandala, E.; Estupiñán-López, F.; Almeraya-Calderón, F. Effect of Heat Treatment on the Electrochemical Behavior of AA2055 and AA2024 Alloys for Aeronautical Applications. *Metals* **2023**, *13*, 429. [CrossRef]
70. Cabral Miramontes, J.A.; Barceinas Sánchez, J.D.O.; Almeraya Calderón, F.; Martínez Villafañe, A.; Chacón Nava, J.G. Effect of Boron Additions on Sintering and Densification of a Ferritic Stainless Steel. *J. Mater. Eng. Perform.* **2010**, *19*, 880–884. [CrossRef]
71. Montoya-Rangel, M.; de Garza-Montes, O.N.; Gaona-Tiburcio, C.; Colás, R.; Cabral-Miramontes, J.; Nieves-Mendoza, D.; Maldonado-Bandala, E.; Chacón-Nava, J.; Almeraya-Calderón, F. Electrochemical Noise Measurements of Advanced High-Strength Steels in Different Solutions. *Metals* **2020**, *10*, 1232. [CrossRef]
72. Tian, H.; Sun, F.; Chu, F.; Wang, L.; Wang, X.; Cui, X. Passivation behavior and surface chemistry of 316 SS in the environment containing Cl^- and NH_4. *J. Electroanal. Chem.* **2021**, *886*, 115138. [CrossRef]
73. Moradi, M.; Rezaei, M. Electrochemical noise analysis to evaluate the localized anti-corrosion properties of PP/graphene oxide nanocomposite coatings. *J. Electroanal. Chem.* **2022**, *921*, 116665. [CrossRef]

74. Xia, D.; Ji, Y.; Zhang, R.; Mao, Y.; Behnamian, Y.; Hu, W.; Birbilis, N. On the localized corrosion of AA5083 in a simulated dynamic seawater/air interface—Part 1: Corrosion initiation mechanism. *Corros. Sci.* **2023**, *213*, 110985. [CrossRef]
75. Deng, C.M.; Xia, D.; Zhang, R.; Behnamian, Y.; Hu, W.; Birbilis, N. On the localized corrosion of AA5083 in a simulated dynamic seawater/air interface—Part 2: Effects of wetting time. *Corros. Sci.* **2023**, *221*, 111367. [CrossRef]
76. Zhu, A.; Zhang, Q.; Liu, P.; Zhang, J.; Cao, F. Quasi-simultaneous electrochemical/chemical imaging of local Fe2+ and pH distributions on 316 L stainless steel surface. *J. Electroanal. Chem.* **2020**, *871*, 114107. [CrossRef]
77. Duan, Z.; Man, C.; Dong, C.; Cui, Z.; Kong, D.; Wang, L.; Wang, X. Pitting behavior of SLM 316L stainless steel exposed to chloride environments with different aggressiveness: Pitting mechanism induced by gas pores. *Corros. Sci.* **2020**, *67*, 108520. [CrossRef]
78. Choudhary, S.; Qiu, Y.; Thomas, S.; Birbilis, N. Element-resolved electrochemical analysis of transpassive dissolution and repassivation behavior of the multi-principal element alloy AlTiVCr. *Electrochim. Acta* **2020**, *362*, 137104. [CrossRef]
79. Li, Z.X.; Zhang, L.M.; Udoh, I.I.; Ma, A.L.; Zheng, Y.G. Deformation-induced martensite in 304 stainless steel during cavitation erosion: Effect on passive film stability and the interaction between cavitation erosion and corrosion. *Tribol. Int.* **2022**, *167*, 107422. [CrossRef]
80. Zhang, L.; Qi, L.; Deng, S.; Oguntuase, O.; Deng, T.; Wang, H.; Ojo, A. Analyses of Anodically Formed Passive Film and Corrosion Behavior of Wire-arc Additive Manufactured ATI 718Plus® Superalloy. *Addit. Manuf.* **2021**, *48*, 102443. [CrossRef]
81. Messinese, E.; Casanova, L.; Paterlini, L.; Capelli, F.; Bolzoni, F.; Ormellese, M.; Brenna, A. A Comprehensive Investigation on the Effects of Surface Finishing on the Resistance of Stainless Steel to Localized Corrosion. *Metals* **2022**, *12*, 1751. [CrossRef]
82. Vodárek, V.; Rožnovská, G.; Kuboň, Z.; Volodarskaja, A.; Palupčíková, R. The Effect of Long-Term Ageing at 475 °C on Microstructure and Properties of a Precipitation Hardening MartensiticStainless Steel. *Metals* **2022**, *12*, 1643. [CrossRef]
83. Ueda, M.; Ikeda, A. Effect of Microstructure and Cr content in steel on CO_2 Corrosion. In Proceedings of the Corrosion/1996, Denver, CO, USA, 24–29 March 1996; Paper No. 96013; NACE: Houston, TX, USA, 1996.
84. Esmaeely, S.N.; Choi, Y.S.; Young, D.; Nesic, S. Effect of calcium on the formation and protectives of iron carbonate layer in CO_2 corrosion. *Corrosion* **2013**, *69*, 912–920. [CrossRef]
85. Keddam, M.; Mattos, O.; Takenouti, H. Mechanism of anodic dissolution of iron-chromium alloys investigated by electrode impedances-II. Elaboration of the reaction model. *Electrochim. Acta* **1986**, *31*, 1159–1165. [CrossRef]
86. Gao, K.W.; Yu, F.; Pang, X.L.; Zhang, G.A.; Qiao, L.J.; Chu, W.Y.; Lu, M.X. Mechanical properties of CO_2 corrosion product scales and their relationship to corrosion rates. *Corros. Sci.* **2008**, *50*, 2796–2803. [CrossRef]
87. Wang, M.; Wu, S.; Wang, P.; Dong, B.; Ma, M.; Zhao, W.; Zhong, J.; Li, H.; Hou, D. Nano-deterioration of steel passivation film: Chloride attack in material defects. *Mater. Struct.* **2023**, *56*, 35. [CrossRef]
88. Jin, Z.; Xiong, C.; Zhao, T.; Du, Y.; Zhang, X.; Li, N.; Yu, Y.; Wang, P. Passivation and depassivation properties of Cr-Mo alloyed corrosion-resistant steel in simulated concrete pore solution. *Cem. Concr. Compos.* **2022**, *126*, 104375. [CrossRef]
89. Mundra, S.; Provis, J.L. Mechanisms of passivation and chloride-induced corrosion of milsteel in sulfide-containing alkaline solutions. *J. Mater. Sci.* **2021**, *56*, 14783. [CrossRef]
90. Buchanan, A.R.; Stansbury, E.E. Chapter 4—Electrochemical Corrosion. In *Handbook of Environmental Degradation of Materials*, 2nd ed.; Elsevier Inc.: Amsterdam, The Netherlands, 2012; Volume 1, pp. 87–125. [CrossRef]
91. Betova, I.; Bojinov, M.; Laitinen, T.; Mäkelä, K.; Pohjanne, P.; Saario, T. The transpassive dissolution mechanism of highly alloyed stainless steels: I. Experimental results and modelling procedure. *Corros. Sci.* **2002**, *44*, 2675–2697. [CrossRef]
92. Fattah-alhosseini, A.; Saatchi, A.; Golozar, M.A.; Raeissi, K. The transpassive dissolution mechanism of 316L stainless steel. *Electrochim. Acta* **2009**, *54*, 3645–3650. [CrossRef]
93. Montoya-Rangel, M.; Garza-Montes-de-Oca, N.; Gaona-Tiburcio, C.; Almeraya-Calderón, F. Corrosion mechanism of advanced high strength dual-phase steels by electrochemical noise analysis in chloride solutions. *Mater. Today Commun.* **2023**, *35*, 105663. [CrossRef]
94. Bojinov, M.; Betova, I.; Fabricius, G.; Laitinen, T.; Saario, T. The stability of the passive state of iron–chromium alloys in sulphuric acid solution. *Corros. Sci.* **1999**, *41*, 1557–1584. [CrossRef]
95. Núñez-Jaquez, R.E.; Buelna-Rodríguez, J.E.; Barrios-Durstewitz, C.P.; Gaona-Tiburcio, C.; Almeraya-Calderón, F. Corrosion of modified concrete with sugar cane bagasse ash. *Int. J. Corros.* **2012**, *2012*, 451864. [CrossRef]
96. Bojinov, M.; Fabricius, G.; Kinnunen, P.; Laitinen, T.; Mäkelä, K.; Saario, T.; Sundholm, G. The mechanism of transpassive dissolution of Ni–Cr alloys in sulphate solutions. *Electrochim. Acta* **2000**, *45*, 2791–2802. [CrossRef]
97. Huang, J.; Wu, X.; Han, E.H. Electrochemical properties and growth mechanism of passive films on Alloy 690 in high-temperature alkaline environments. *Corros. Sci.* **2010**, *52*, 3444–3452. [CrossRef]
98. Calinski, C.; Strehblow, H.H. ISS depth profiles of the passive layer on Fe/Cr alloys. *J. Electrochem. Soc.* **1989**, *36*, 1328–1331. [CrossRef]
99. Martínez-Ramos, C.; Olguin-Coca, J.; Lopez-Leon, L.D.; Gaona-Tiburcio, C.; Lara-Banda, M.; Maldonado-Bandala, E.; Castañeda-Robles, I.; Jaquez-Muñoz, J.M.; Cabral-Miramontes, J.; Nieves-Mendoza, D.; et al. Electrochemical Noise Analysis Using Experimental Chaos Theory, Power Spectral Density and Hilbert–Huang Transform in Anodized Aluminum Alloys in Tartaric–Phosphoric–Sulfuric Acid Solutions. *Metals* **2023**, *13*, 1850. [CrossRef]
100. Li, J.; Lin, B.; Zheng, H.; Wang, Y.; Zhang, H.; Zhang, Y.; Nie, Z.; Tang, J. Study on pitting corrosion behavior and semi in-situ pitting corrosion growth model of 304 L SS with elastic stress in NaCl corrosion environment. *Corros. Sci.* **2023**, *211*, 110862. [CrossRef]

101. Tranchida, G.; Clesi, M.; Franco, F.D.; Quarto, F.D.; Santamaria, M. Electronic properties and corrosion resistance of passive films on austenitic and duplex stainless steels. *Electrochim. Acta* **2018**, *273*, 412–423. [CrossRef]
102. Ma, L.; Pascalidou, E.M.; Wiame, F.; Zanna, S.; Maurice, V.; Marcus, P. Passivation mechanisms and pre-oxidation effects on model surfaces of FeCrNi austenitic stainless steel. *Corros. Sci.* **2020**, *167*, 108483. [CrossRef]
103. Doh, S.J.; Je, J.H.; Kim, J.S.; Kim, K.Y.; Kim, H.S.; Lee, Y.D.; Lee, J.M.; Hwu, Y. Influence of Cr and Mo on the passivation of stainless steel430 (18Cr) and 444 (18Cr–2Mo): In situ XANES study. *Nucl. Instrum. Meth. B* **2003**, *199*, 211–215. [CrossRef]
104. Fattah-alhosseini, A.; Taheri Shoja, S.; Heydari Zebardast, B.; Mohamadian Samim, P. An Electrochemical Impedance Spectroscopic Study of the Passive State on AISI 304 Stainless Steel. *Int. J. Electrochem.* **2011**, *2011*, 152143. [CrossRef]
105. Castro, B.E.; Vilche, R.J. Investigation of passive layers on iron and iron-chromium alloys by electrochemical impedance spectroscopy. *Electrochim. Acta* **1993**, *38*, 1567–1572. [CrossRef]
106. Zhi-Gang, L.; Yi, Z.; Huan, W.; Shan, W.; Long-Fei, S.; Bo-Kai, L.; Xing-Peng, G. Modified nano-lignin as a novel biomass-derived corrosion inhibitor for enhanced corrosion resistance of carbon steel. *Corros. Sci.* **2024**, *227*, 111705. [CrossRef]
107. Alireza, R.; Abdolreza, F.; Avni, B.; Alireza, S.; Mikhail, A.V.; Valbonë, M.; Xiankang, Z.; Samira, Y.; Richard, D. Novel sucrose derivative as a thermally stable inhibitor for mild steel corrosion in 15% HCl medium: An experimental and computational study. *Chem. Eng. J.* **2022**, *446*, 136938. [CrossRef]
108. Martínez-Villafañe, A.; Almeraya-Calderón, M.F.; Gaona-Tiburcio, C.; Gonzalez-Rodriguez, J.G.; Porcayo-Calderón, J. High-Temperature Degradation and Protection of Ferritic and Austenitic Steels in Steam Generators. *J. Mater. Eng. Perform.* **1998**, *7*, 108–113. [CrossRef]
109. Jinlong, L.; Tongxiang, L.; Chen, W.; Limin, D. Comparison of corrosion properties of passive films formed on coarse grained and ultrafine grained AISI 2205 duplex stainless steels. *J. Electroanal. Chem.* **2015**, *757*, 263–269. [CrossRef]
110. Yang, G.; Du, Y.; Chen, S.; Ren, Y.; Ma, Y. Effect of secondary passivation on corrosion behavior and semiconducting properties of passive film of 2205 duplex stainless steel. *J. Mat. Res. Technol.* **2021**, *15*, 6828. [CrossRef]
111. Cai, Y.; Zheng, H.; Hu, X.; Lu, X.; Lu, J.; Poon, C.; Li, W. Comparative studies on passivation and corrosion behavior of two types of steel bar in simulated concrete pore solution. *Const. Buld. Mater.* **2021**, *266*, 120971. [CrossRef]
112. SHen, Z. The influence of Cr and Mo on the formation of the passivation film on the surface of ferritic stainless steel. *Mater. Commun. Today* **2024**, *38*, 108221. [CrossRef]